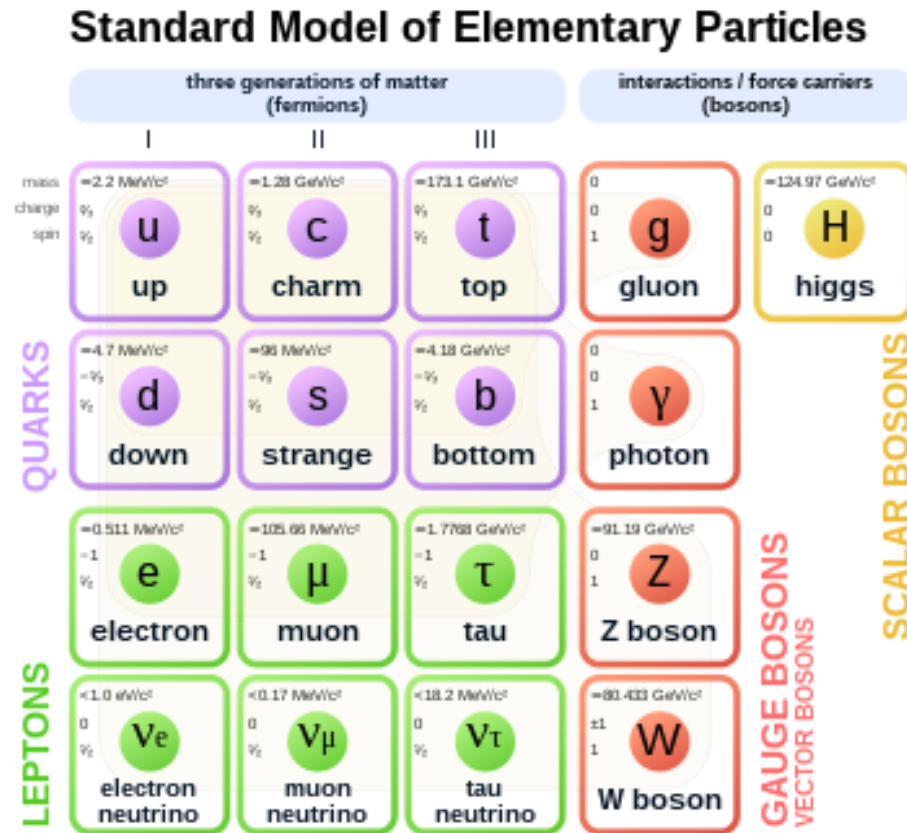


Searching for Non-Standard Model Highly Ionizing Processes and Long- Lived Neutral Particles With the MoEDAL-MAPP Detector

Alejandro Salazar Lobos

Beyond the Standard Model

- The Standard Model (SM) describes the behaviour of all elementary particles and their interactions
- Last piece of the SM: Higgs Boson (2012)

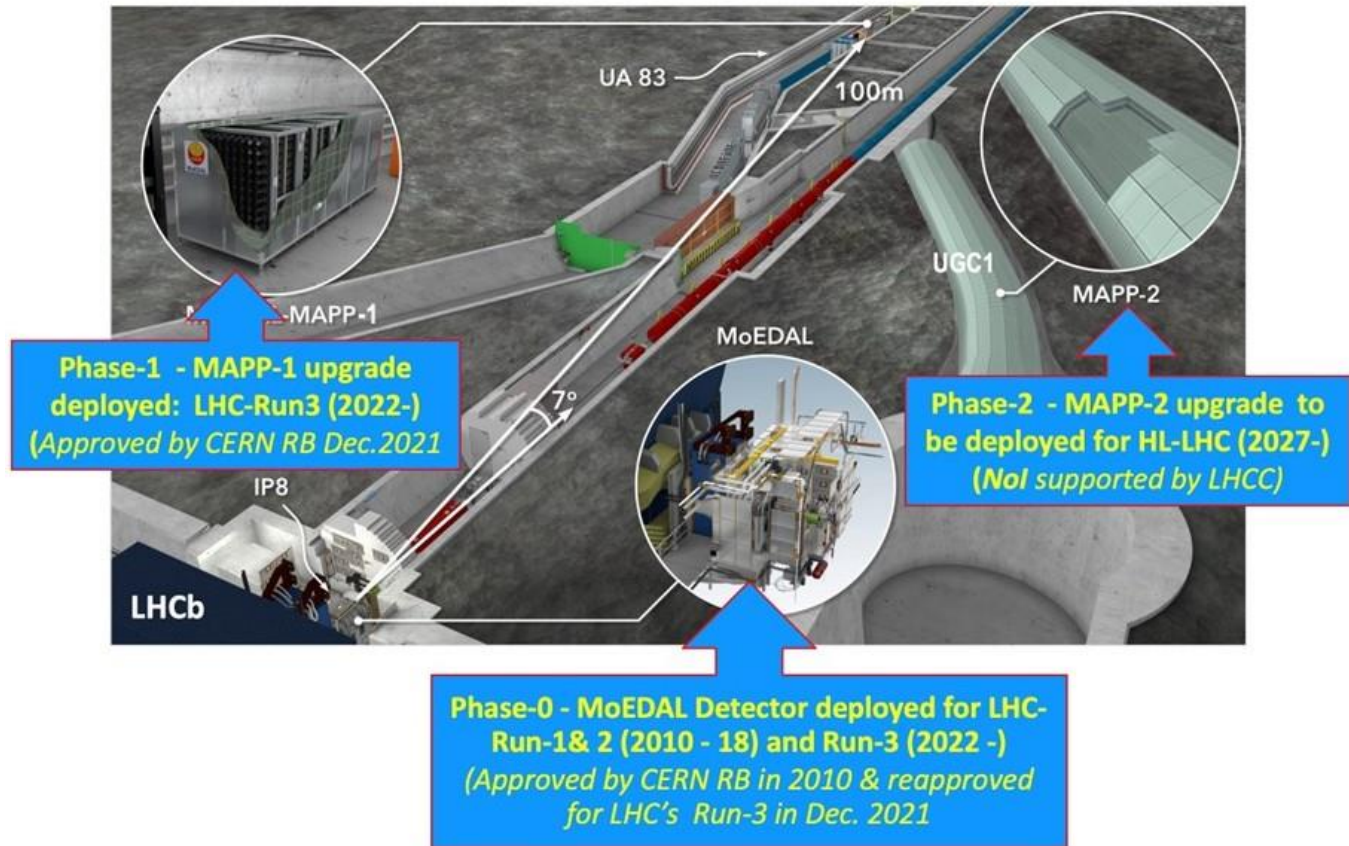


Retrieved from:
https://en.wikipedia.org/wiki/Standard_Model

- Limitations:
 - 1) ~24 experimental parameters?
 - 2) Neutrino masses?
 - 3) Imbalance between matter and anti-matter?
 - 4) Presence of dark matter and dark energy?
 - 5) Incorporation of a theory of gravity (General Relativity)?

MoEDAL-MAPP

- 2010 - Monopole and Exotics Detector at the LHC (MoEDAL) (HIPs)
 - First dedicated search detector (new class of detector at the LHC)
 - Passive detector
- 2021 – MoEDAL Apparatus for Penetrating Particles – Phase 1 (MAPP-1) (mCPs; other FIPs, such as particles with large EDMs, and LLPs)
- 2029 – MAPP – Phase 2 (MAPP-2) (enhance MAPP-1's ability to detect LLPs)



Location of the MAPP detector(s) at the LHC. MAPP is to be installed in the UA83 (Phase-1) and UGC1 (Phase-2) tunnels at the LHC, which is adjacent to the MoEDAL detector

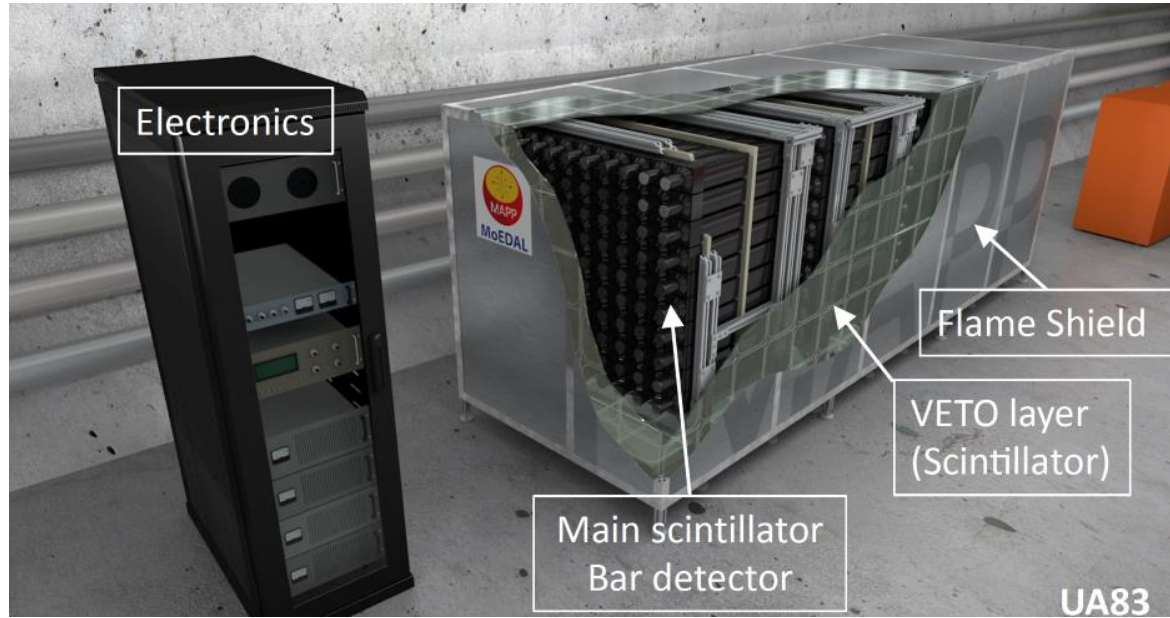
MAPP-1 Motivation

- Expansion of the LHC's discovery horizon: sensitivity to more BSM physics scenarios (mCPs, FIPs, and LLPs)
- Mini-Charged Particles
 - Fractional charges
 - Milli-charged particles could come from dark sector models
- Anomalously Large EDMs
 - A large EDM detected by the MAPP detector would be evidence of new physics [1]

[1] M. Frank, M. de Montigny, P.-P. Ouimet, J.L. Pinfold, A. Shaa, and M. Staelens. "Searching for heavy neutrinos with the MoEDAL-MAPP detector at the LHC". In: *Physics Letters B* 802(2020), p. 135204. Doi: 10.1016/j.physletb.2020.135204

MAPP-1 Detector

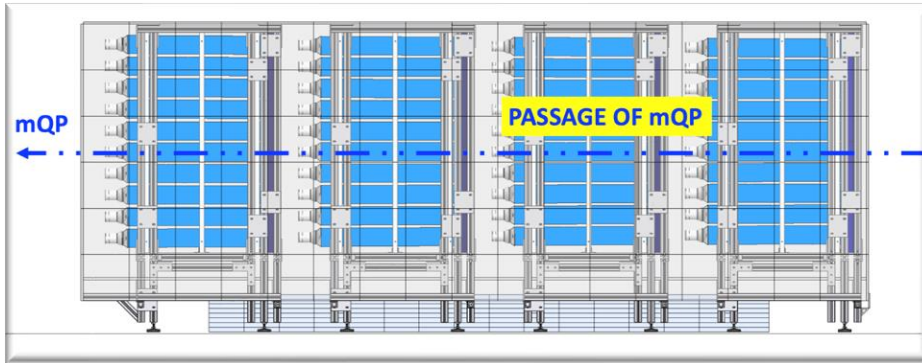
- UA83 gallery (LHC's Run-3) 2022
- Divided into four equal sections, each a 10×10 array of 100 scintillator bars (each bar has a 10 cm by 10 cm cross section and a length of 75 cm)
- 3.1-inch PMT readout (HZC Photonics XP72B22)
- Support structure: HDPE plate matrices
- Frame: T-bar aluminum
- Veto layer encasement + aluminum frame shield



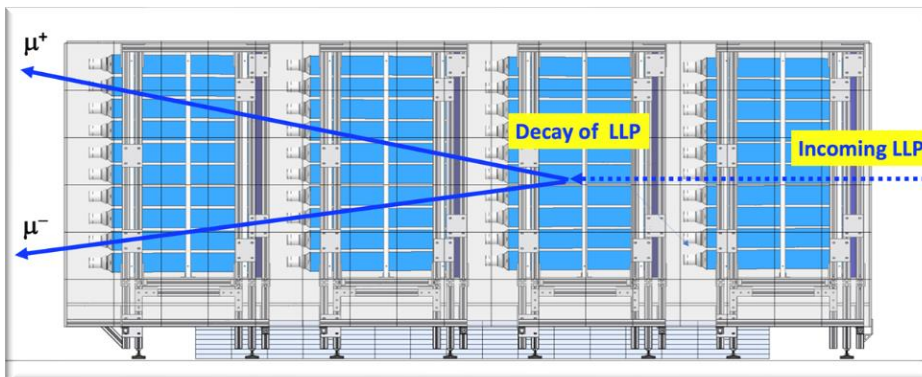
An illustration of the MAPP-1 detector



Muons from IP (Calibration)



Mini-charged particle detection

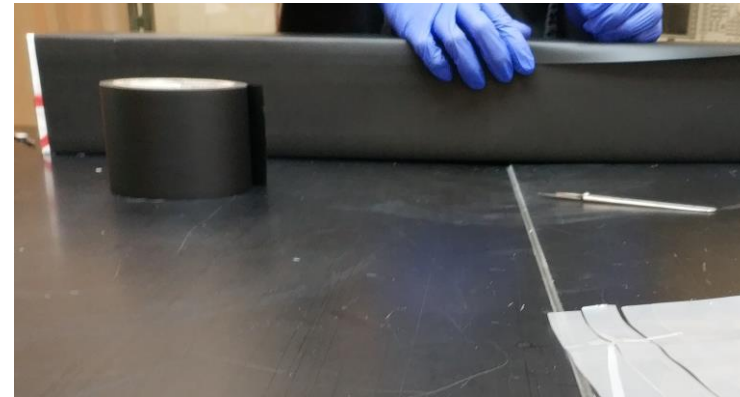


Neutral LLP Detection

A side view of the MAPP detector and different scenarios

MAPP-1 Scintillators

- Scintillator bars make up four collinear with cross-section 1 m^2 (100 10 cm \times 10 cm units, 75 cm length).
- Scintillators developed for high-light emission (doped with 2 % para-Terphenyl and 0.05 % POPOP as secondary fluor) by the MoEDAL group of the Czech Technical University
- Coupling between bar and PMT achieved mechanically via a black plastic housing (injection mold) forming an air-gap-free junction between a rubber light guide (silicon Sylgard 184) and bar
- Readout: 3.1-inch PMTs (HZC Photonics XP72B22)



Wrapping procedure of scintillating units for MAPP-1

MAPP-1 Scintillators (continuation)

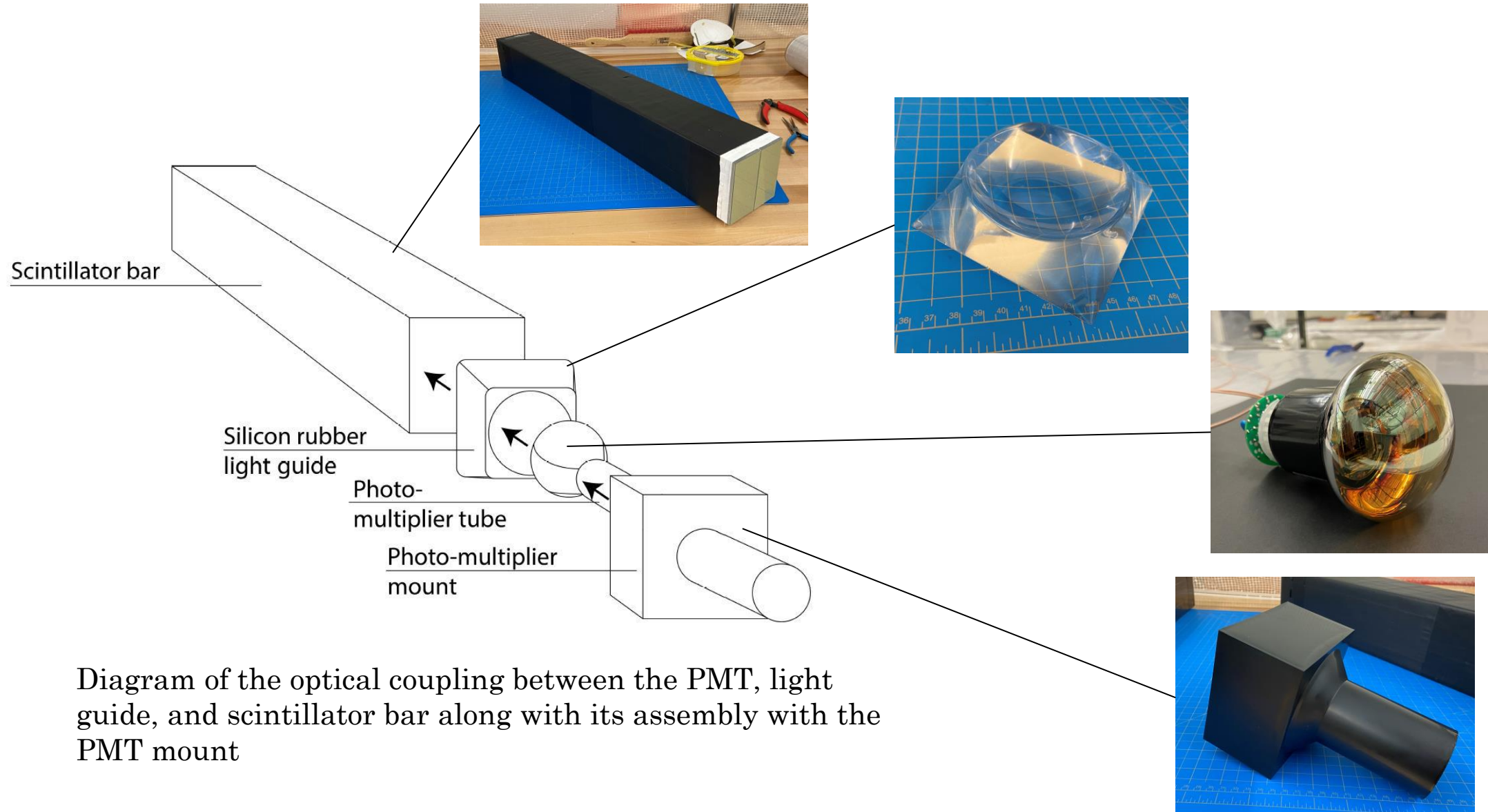


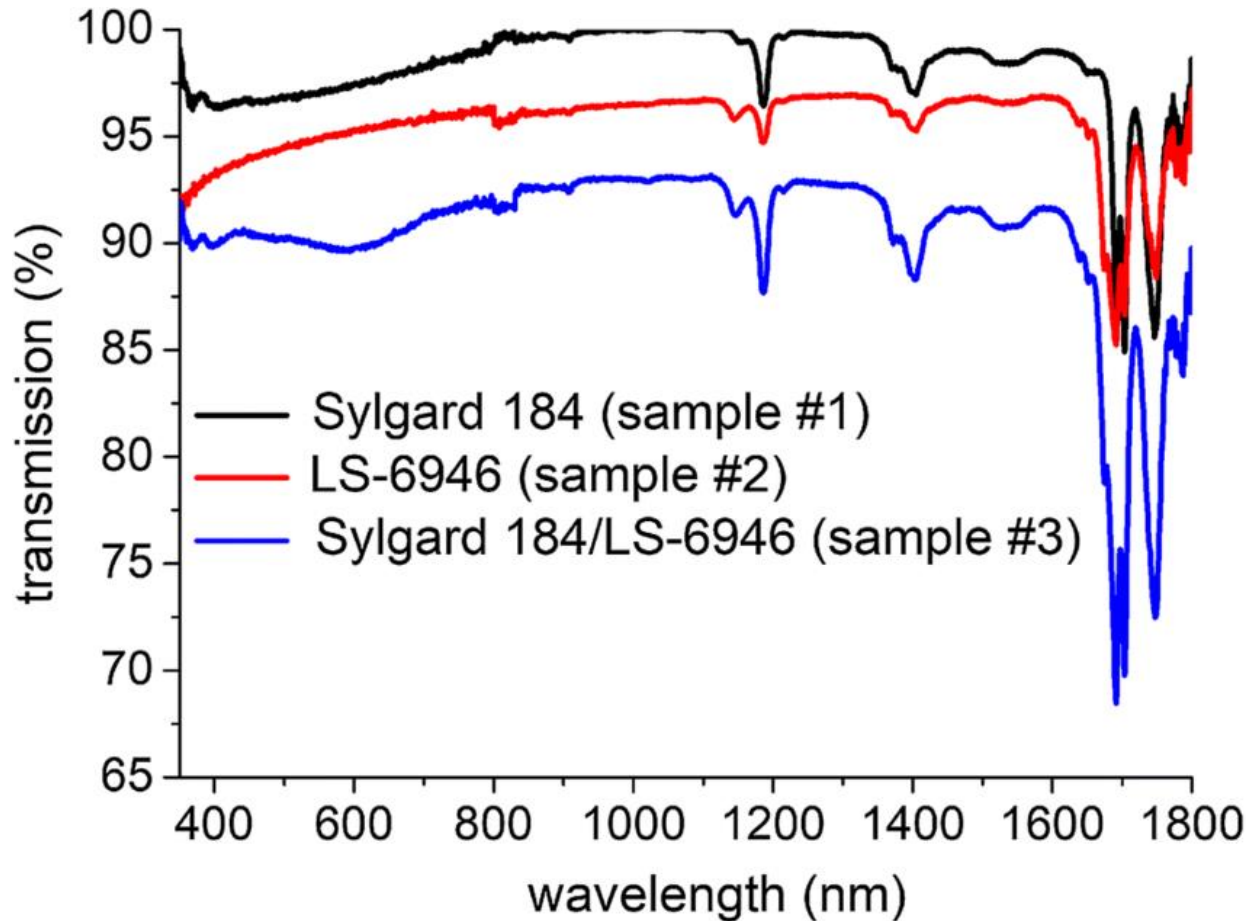
Diagram of the optical coupling between the PMT, light guide, and scintillator bar along with its assembly with the PMT mount

Light-Guides



Silicon rubber (Sylgard 184) light guide and mold

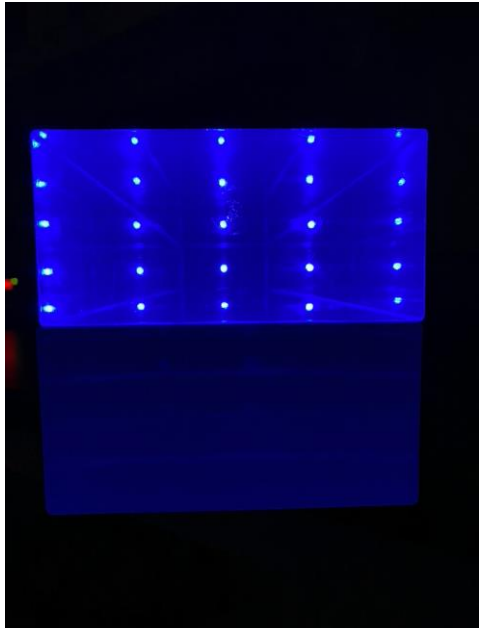
[2] V. Prajzler, M. Neruda, and M. Květoň. "Flexible multimode optical elastomer waveguides". In: Journal of Materials Science: Materials in Electronics 30 (Sept. 2019). Doi: 10.1007/s10854-019-02087-1



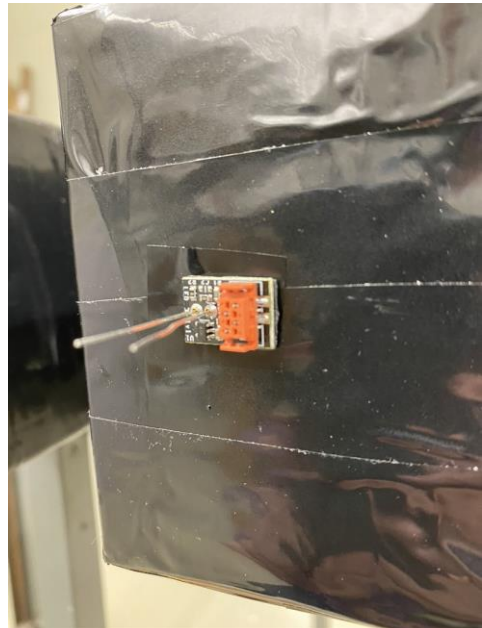
Sylgard 184 transmission efficiency. Taken from [2]

MAPP-1 Scintillator Calibration System

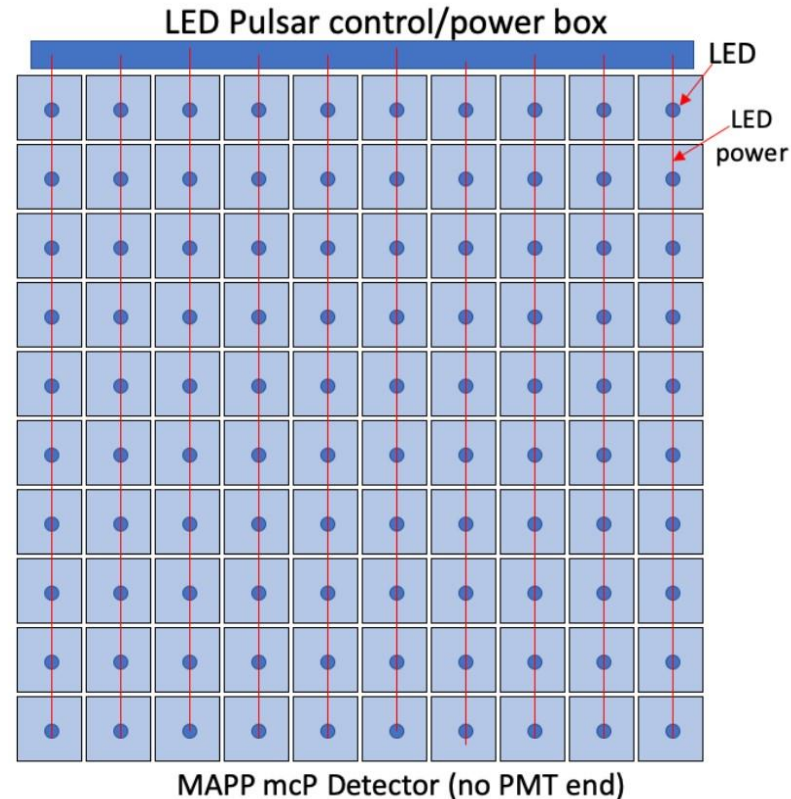
- To test the operation of the MAPP-1 detector, an LED calibration system was installed at the end of the scintillator bars compromising the detector. The LED will be driven by a pulser running at min. 15 ns with a variable voltage. This allows for the simulation of the light expected to be emitted from the interaction of an ionizing particle with the scintillating material



LED on as seen through the bar



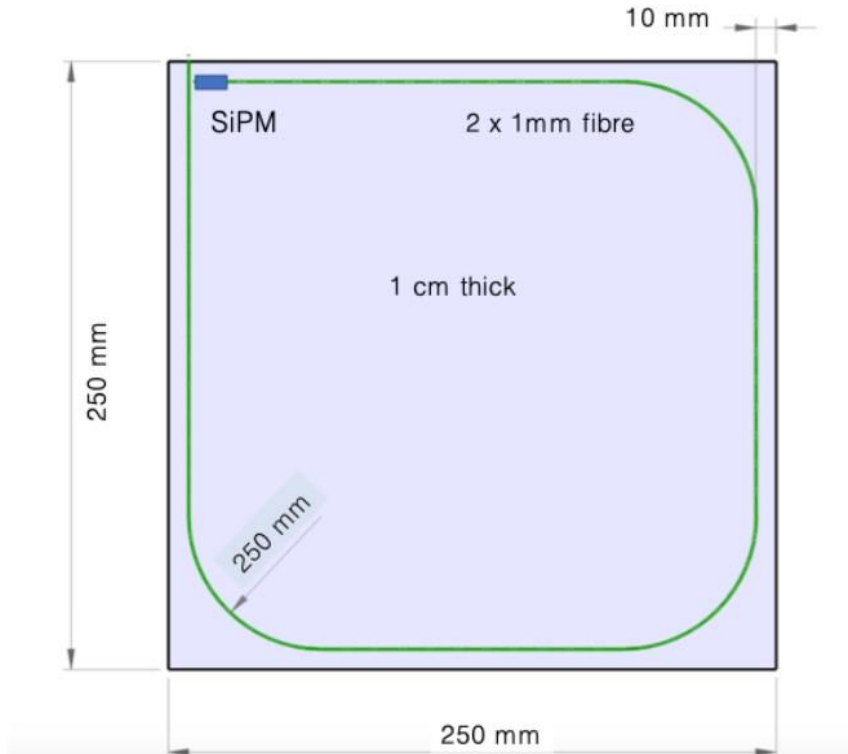
Electronic board installed at wrapped end of scintillating unit



A schematic view of the MAPP-mCP pulser system

The VETO Scintillator-Tile System for MAPP-1

- Veto encasing (25 cm × 25 cm tiles, thickness of 1 cm). Readout: WLS fibres, diameter 1 mm, KETEK PM3225 WB 3 × 3 mm² SiPMs

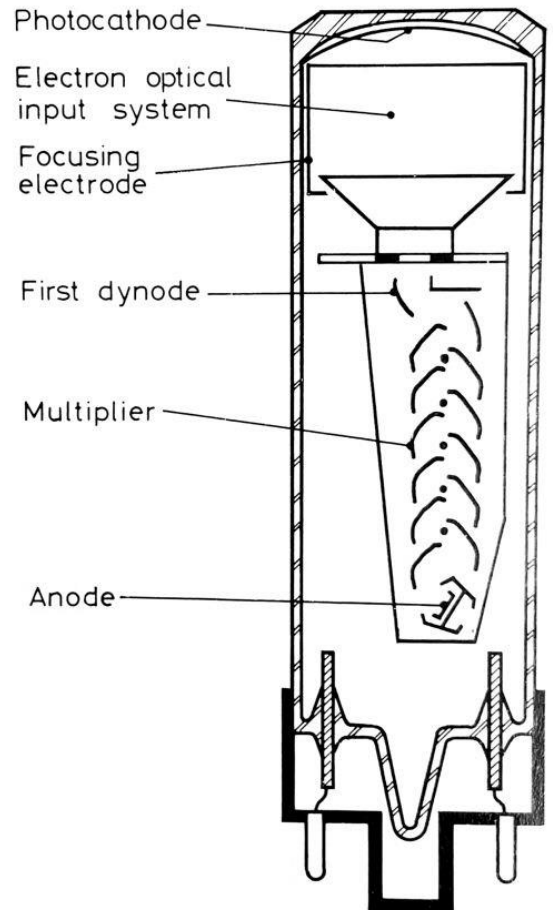


A scintillating tile basic element of the MAPP-1 veto system



Test veto tile

Photomultiplier Tubes for MAPP-1



Basic diagram of the interior of a PMT [3]

[3] W.R. Leo. *Techniques for Nuclear and Particle Physics Experiments - A How-to Approach*. 2nd revised ed. Springer-Verlag

Photomultiplier Tube

**10-stage
80mm (3.1"), Round tube**

Application

✓ Energy physics

Features

✓ High QE
✓ Low background

Description

Window material	Borosilicate low K
Photocathode	Bi-alkali
Refr. Index at 420nm	1.54
Multiplier structure	Box and Linear focused

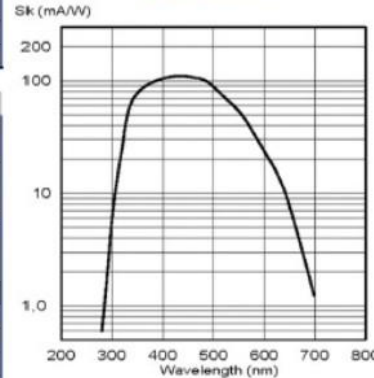
Photocathode characteristics

Spectral range:	Min.	Typ.	Max.	Unit
Maximum sensitivity at		300-550		nm
		404		nm
Sensitivity:				
Luminous		110		µA/lm
Blue *	10	12.5		µA/lmF
Quantum Efficiency at 404 nm *	25			%
Quantum Efficiency at 470 nm *	18			%
Characteristics with voltage divider A	Min.	Typ.	Max.	Unit
Gain slope (vs supp. Volt., log/log)		6.8		
For an anode blue sensitivity of		50		A/lmF
Supply voltage *	900	1150	1300	V
Gain		3x10 ⁶		
Anode dark current		10	30	nA
Dark count *		600	2000	cps
Mean anode sensitivity deviation:				
Long term (18h)		1		%
After change of count rate		1		%
vs temperature between 0 and +40°C at 400 nm		-0.3		%/K
For a supply voltage of: 1000V	Min.	Typ.	Max.	Unit
Linearity (2%) of anode current up to		30		mA
Anode pulse:				
Rise time		3.5		ns
Duration at half height		5		ns
Transit time		49		ns

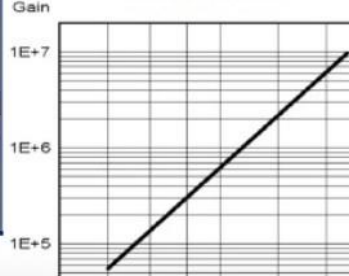
XP72B22



Typical spectral



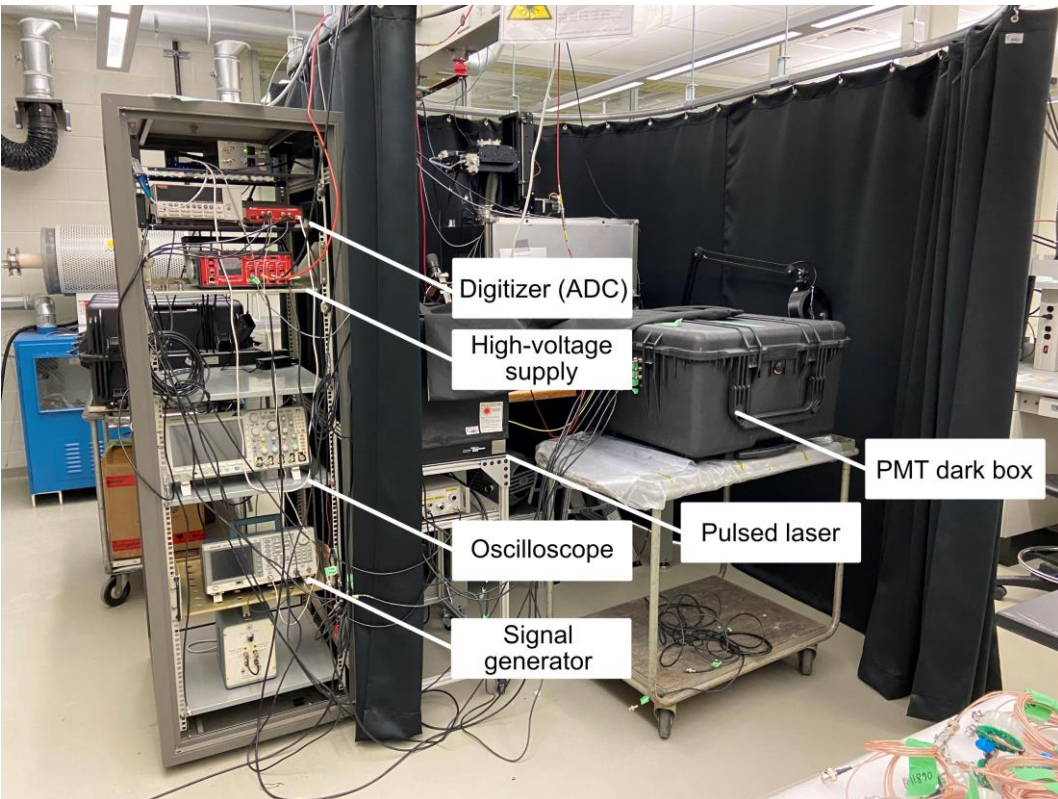
Typical gain curve



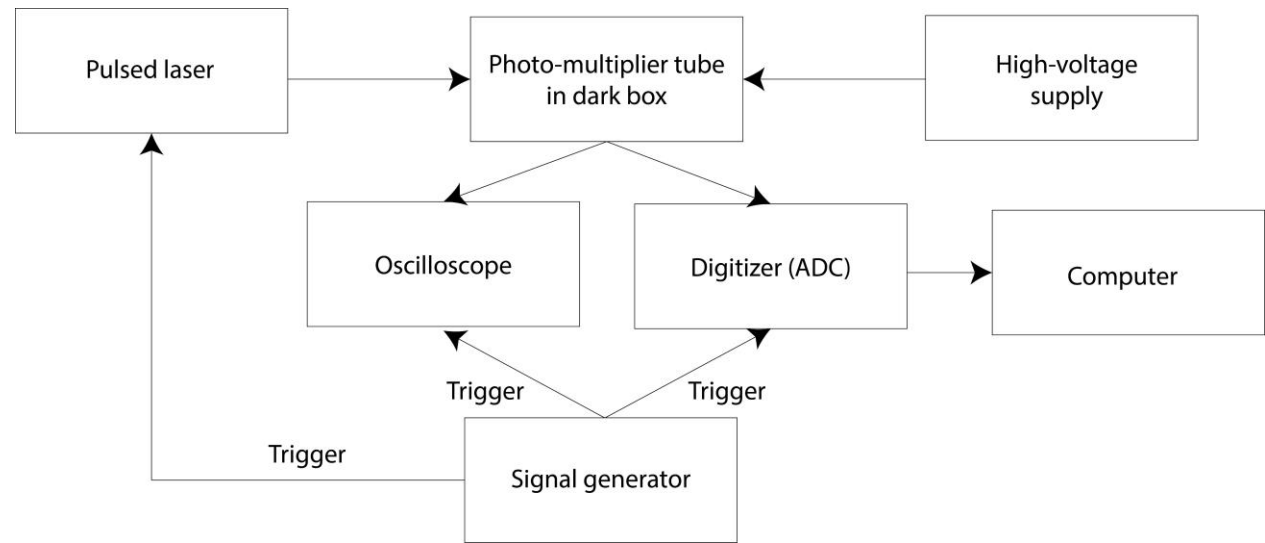
Specifications sheet of the PMTs used in MAPP-1

PMT Testing

- Main purpose: to determine the voltage at which the PMTs should be operated
- Special thanks to Dr. Yanez for letting me use his testing equipment

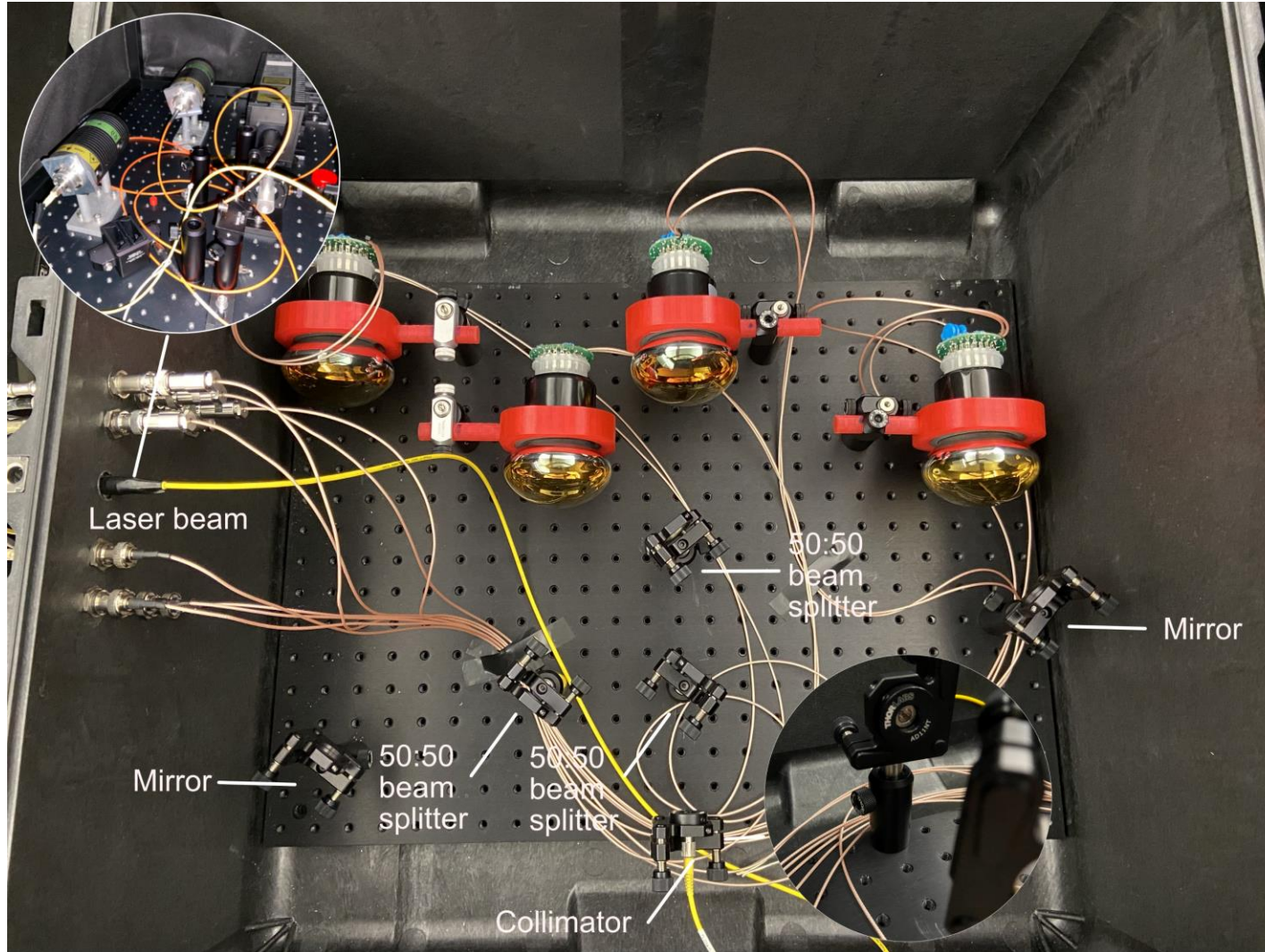


The laser pulser system used to make the measurements



Laser pulser setup diagram

PMT Testing Optical Table Setup

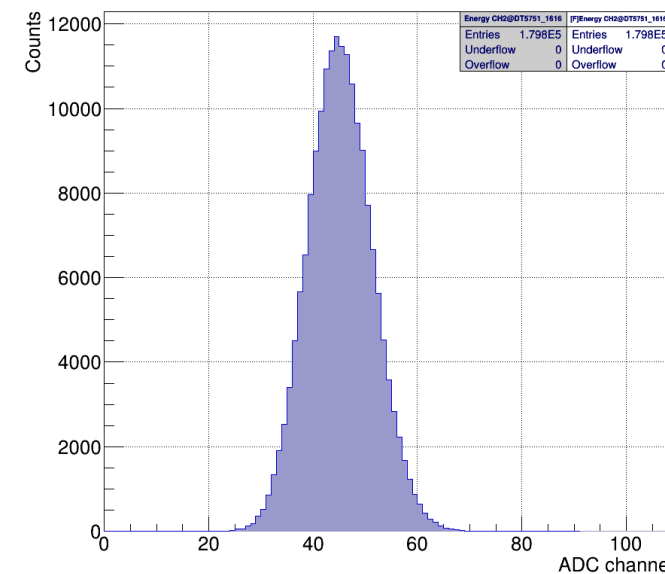


Optical table setup for the testing of PMTs

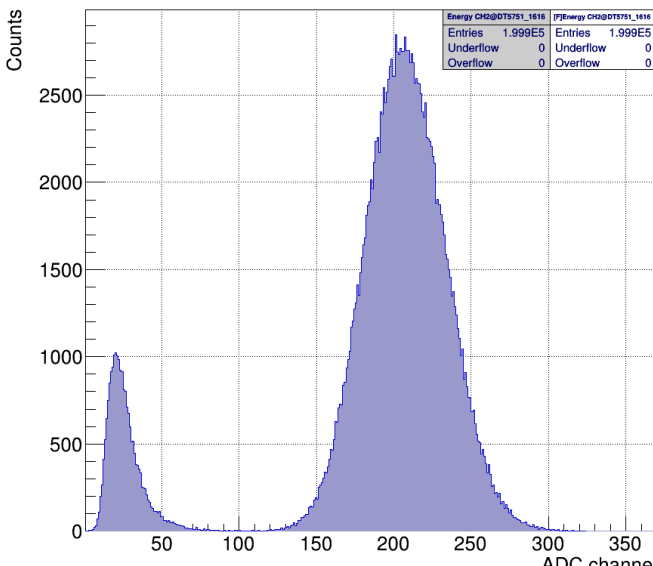
PMT Testing Results



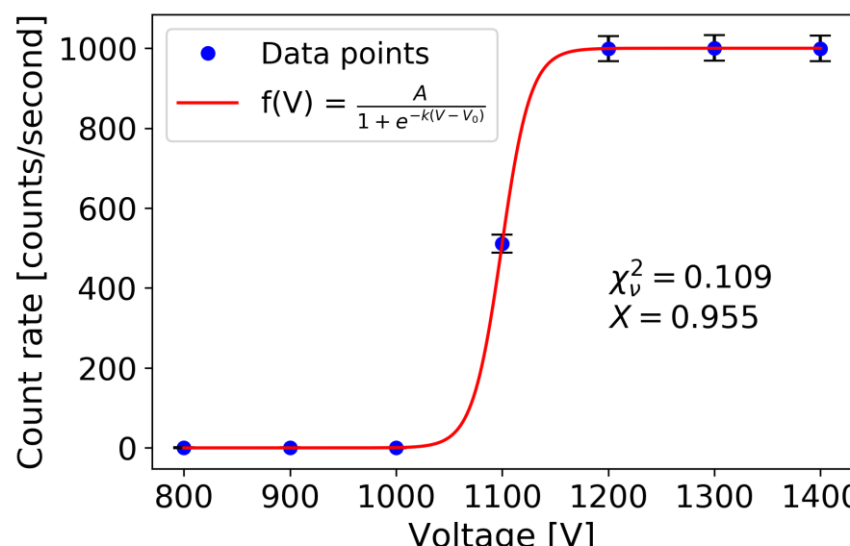
PMT signal (green) within square pulse (yellow)



Sample histogram of tested PMT at 1200 V



PMT tested beyond the plateau region, at 1500 V



Typical count rate curve of a PMT up to the plateau region

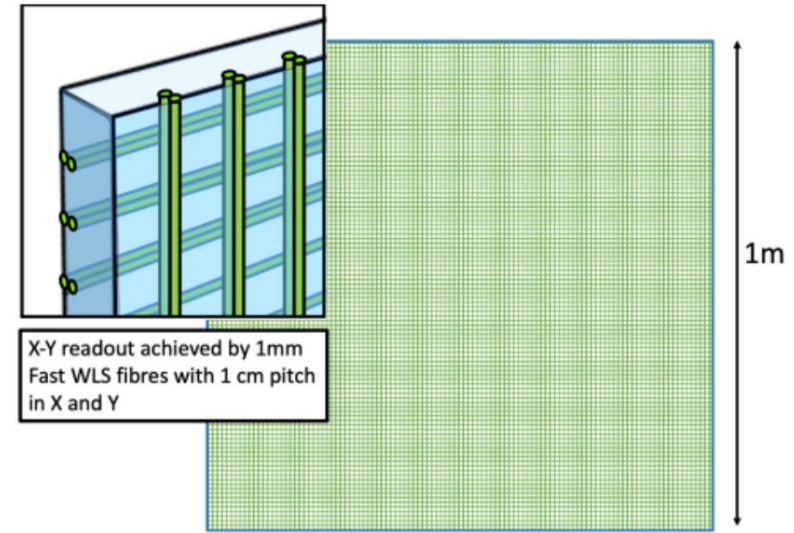
MAPP-2 Motivation

- Expansion of the particle physics horizon to enhance search for LLPs
- Long-Lived Particles
 - Limitations with current general purpose experiments: for ATLAS and CMS the decay vertex occurs outside of the detector [4]

[4] J. Alimena and et. Al. “Searching for long-lived particles beyond the Standard Model at the Large Hadron Collider”. In: *Journal of Physics G: Nuclear and Particle Physics* 47.9 (Sept. 2020), p. 090501. Doi: 10.1088/1361-6471/ab4574

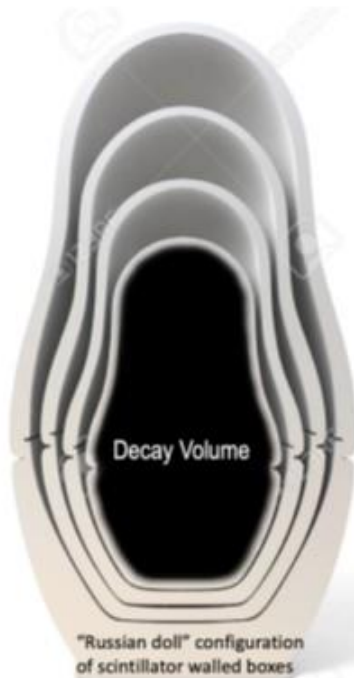
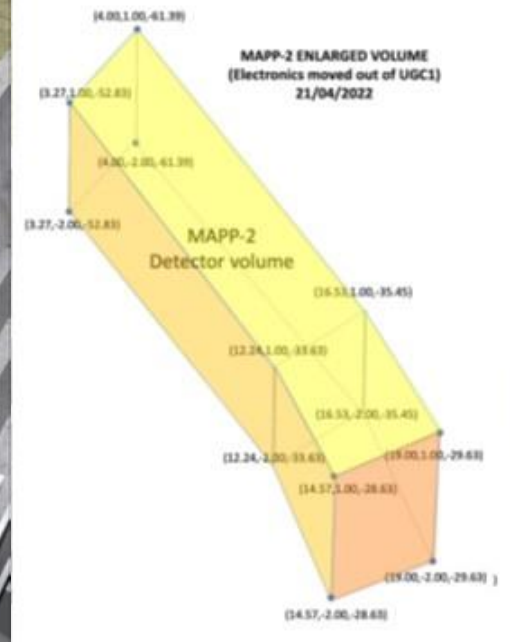
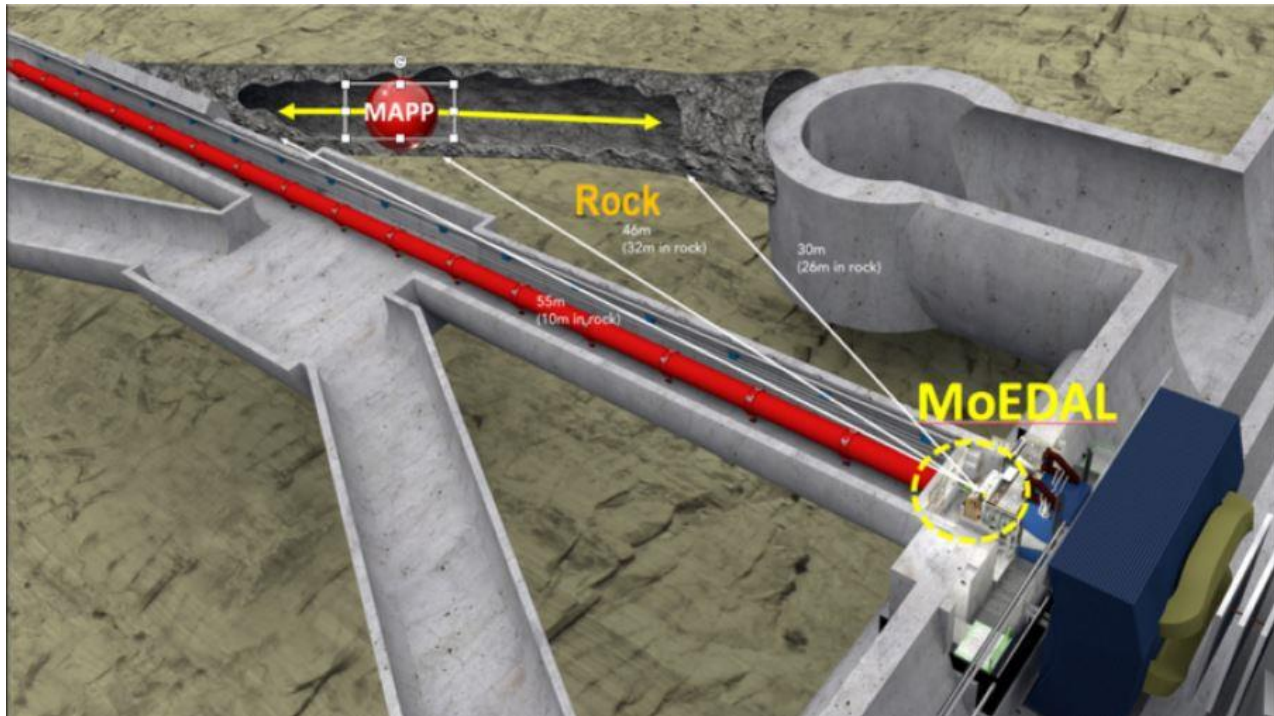
MAPP-2 Detector

- UGC1 Tunnel
- Russian doll geometry lining the tunnel
- $3 \times 3 \text{ mm}^2$ SiPM readout (Ketek PM3315-WB)
- WLS embedded in scintillator (isotropic light re-emission)
- Scintillator sheets follow the geometry of the UGC1 tunnel in a Russian doll fashion. Light is guided via WLS fibres



A visual description of the MAPP-2 detector

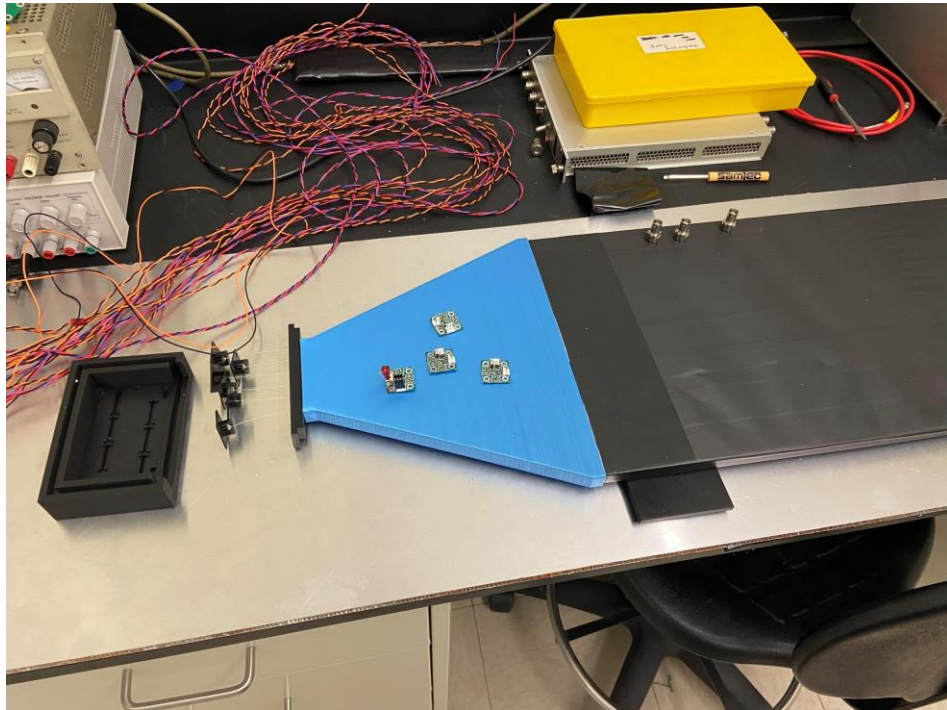
Enhancement to MAPP-1 LLP detection capacity by MAPP-2



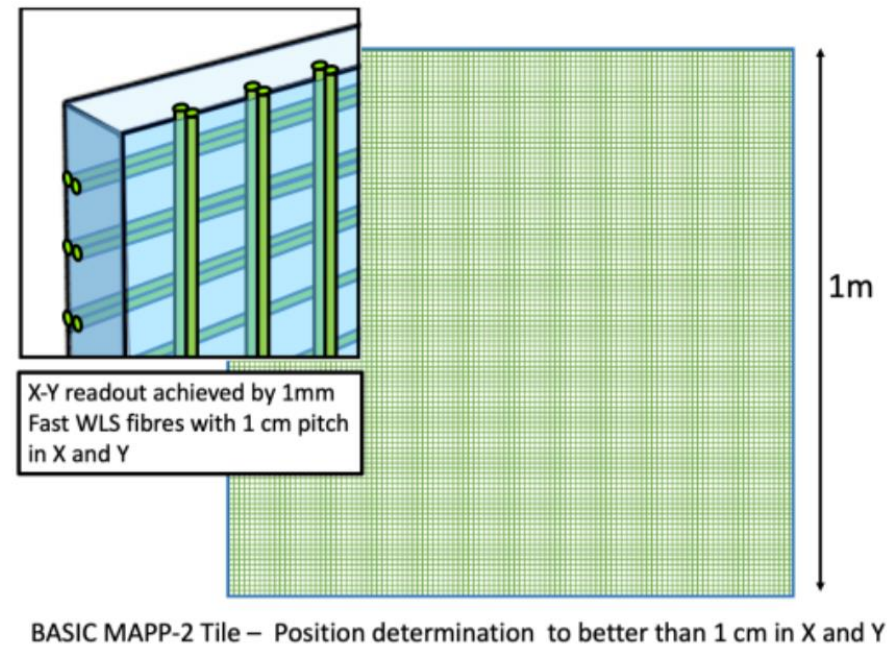
(LEFT) the fiducial volume of the MAPP-2 detector. (RIGHT) the “Russian doll” layout of the nested walls comprising the MAPP-2 detector

Test Tile for MAPP-2

- Main purpose: look at the light transmission efficiency through the bar by scanning it with a 3D plotter using bismuth-207. Scanner precision of about 0.5 mm. Improve tracking resolution



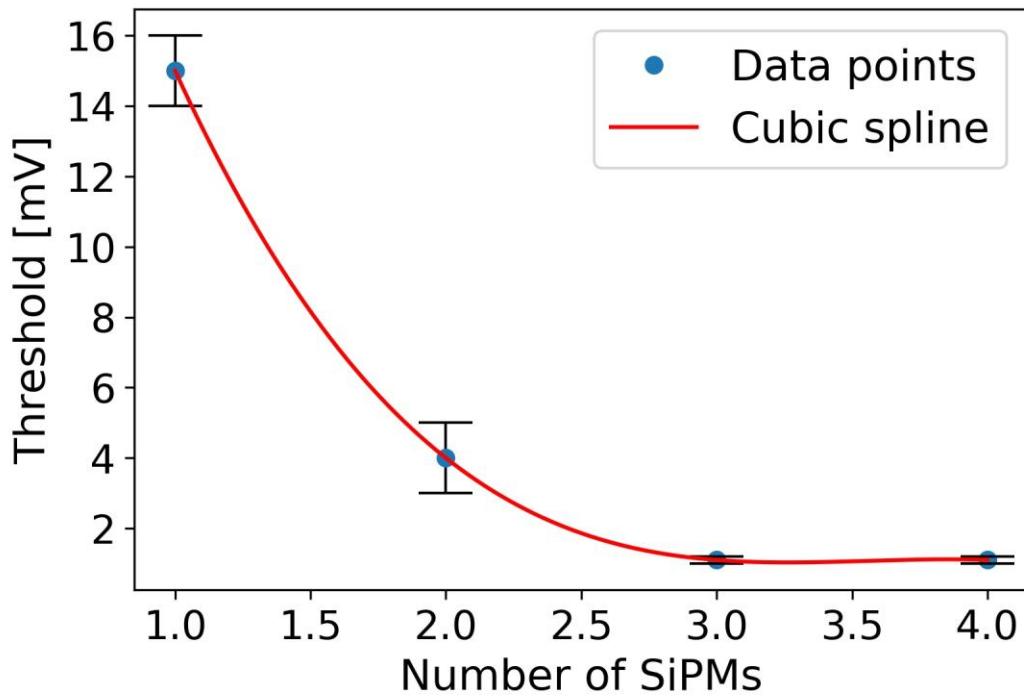
Scintillator tile with parallel optical fibres embedded in it



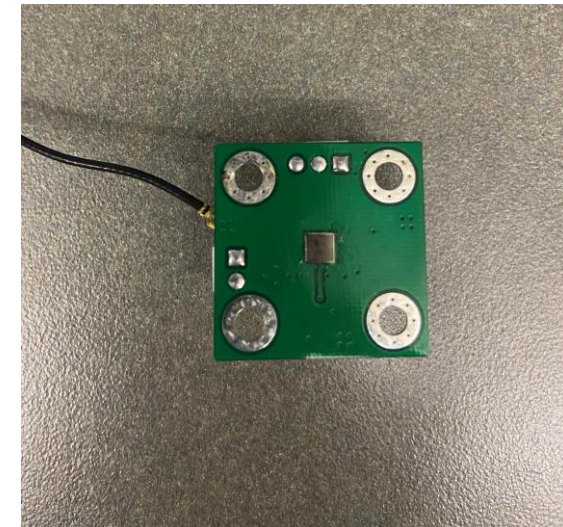
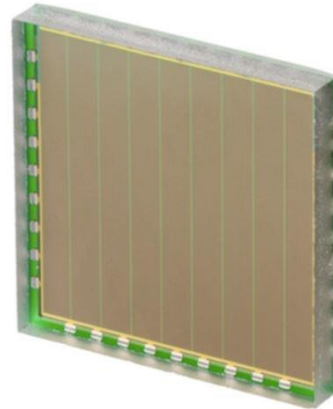
Scintillating tile vision for MAPP-2

Silicon-PM Noise Reduction Testing

- Purpose: to find the optimal amount of SiPMs to place in coincidence at the end of the optical fibres to reduce noise

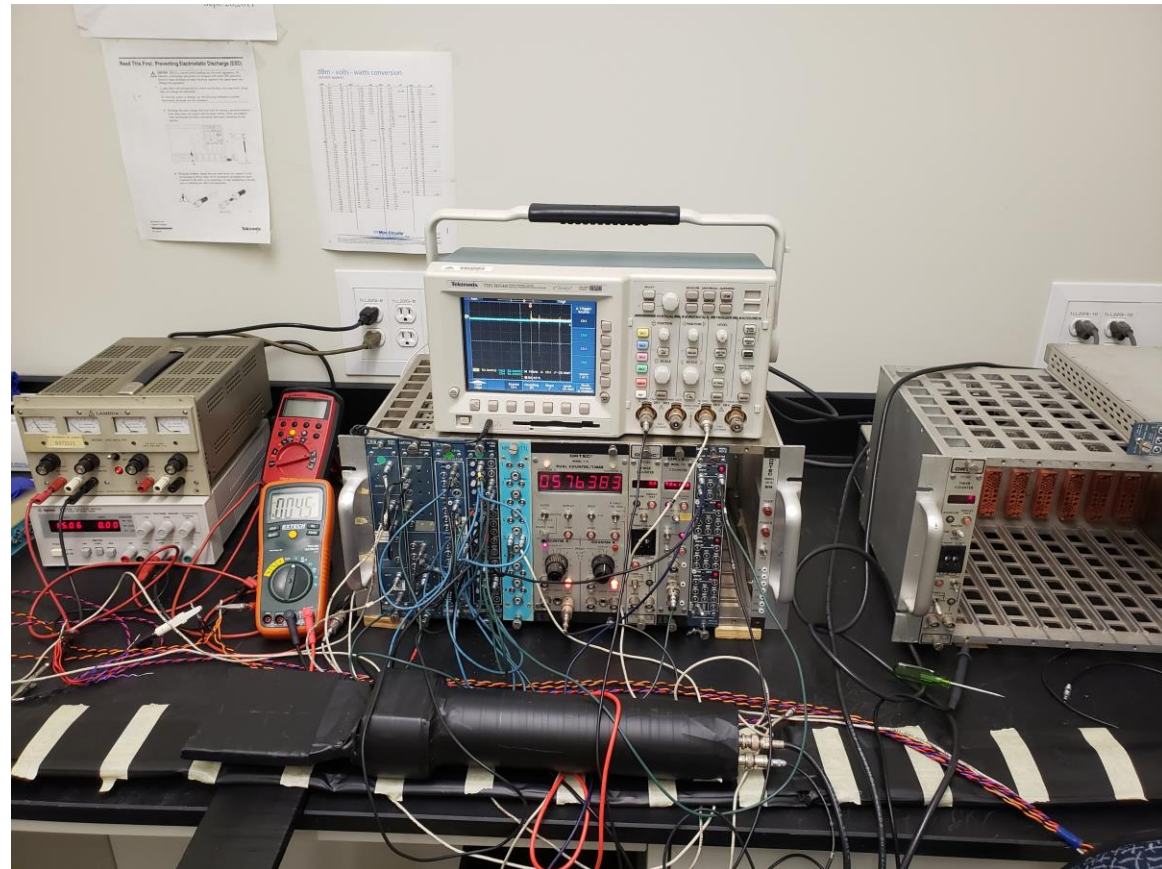
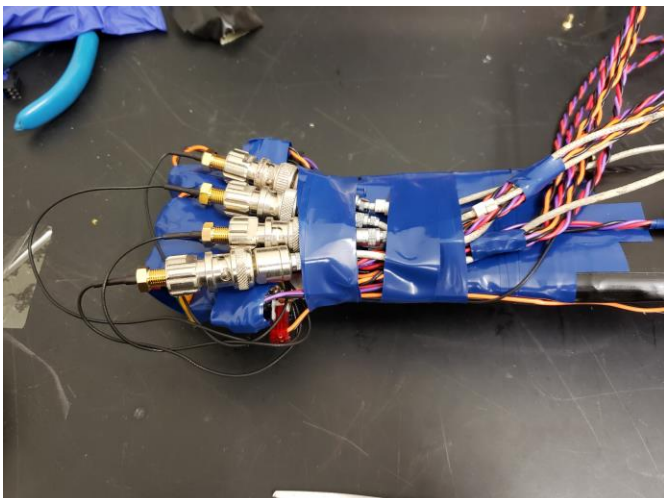
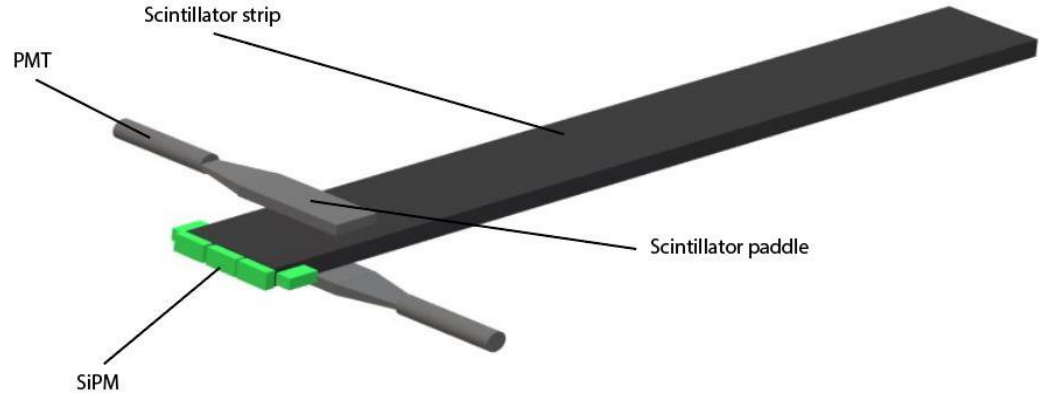


Threshold at which the noise from the SiPMs is killed per number of SiPMs put in coincidence



Ketek PM3315-WB SiPM. Taken from
<https://www.ketek.net/wp-content/uploads/KETEK-PM3315-WBC0-Datasheet.pdf>

Silicon-PM Noise Reduction Testing (continuation)



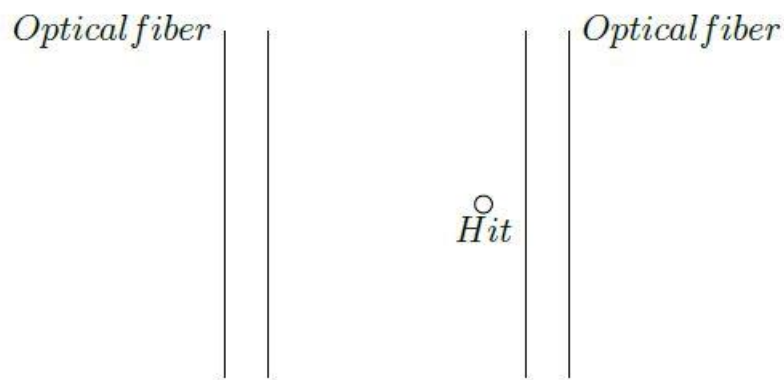
SiPM noise testing setup

Vertex Reconstruction Algorithm for MAPP-2

- Test volume of box within box
- Purpose: determine the detector's potential decay vertex reconstruction capacity and efficiency:

$$\text{Efficiency} = \frac{\# \text{ of correct vertex reconstructions}}{\# \text{ of trials}}$$

- PROCEDURE (approach as detailed in [5]):
 - Generate the decay tracks from the incoming particle
 - Look at the point of intersection between the decay tracks and the detection walls
 - Assign to the an optical fibre coordinate per detection plane to the decay hits



A hit in between two optical fibres means that both fibres are assumed to be hit.

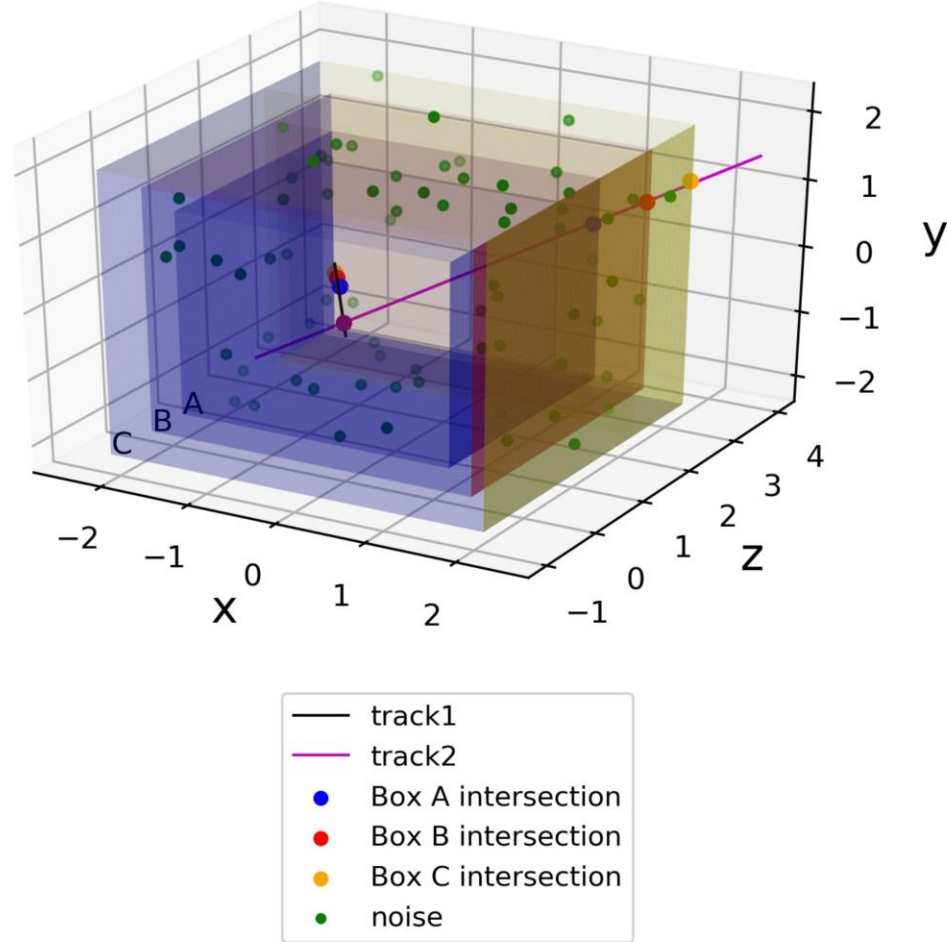


Figure of the three-box test volume.

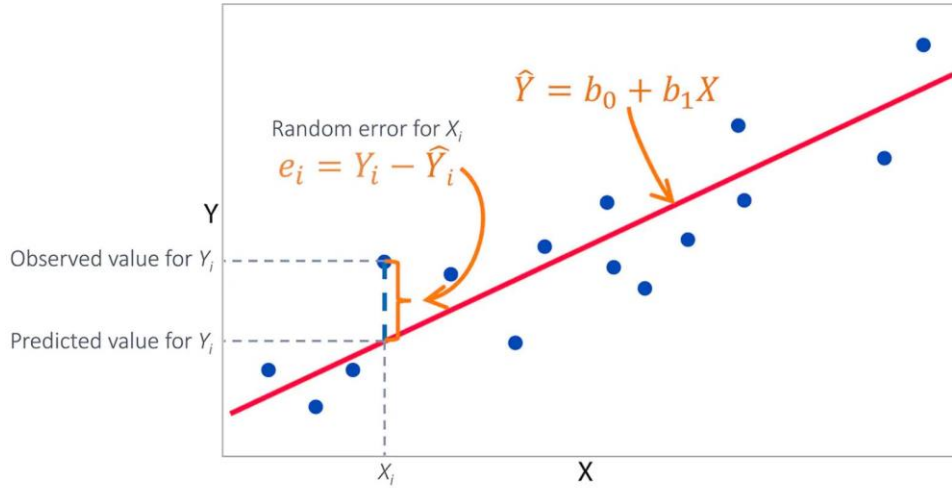
Vertex Reconstruction Algorithm (continuation)

- Combine these coordinates with noise coordinates to blind the code, momentarily (matrix technique)
- For all the coordinates in the detection walls, generate lines via a least-squares fit
- For all the generated lines, run a goodness of fit test: chi-squared

$$\chi^2 = \sum_i \frac{(C_{predicted} - C_{observed})_i^2}{\sigma_{observed_i}^2}$$

$$X(\chi^{2'}; \nu) = \int_{\chi^{2'}=\chi^2}^{\chi^{2'} \rightarrow \infty} \frac{\chi^{2' \nu/2 - 1} \exp(-\chi^{2'}/2)}{2^{\nu/2} \Gamma(\nu/2)} d\chi^{2'}$$

- Best chi-square results: ≤ 0.5
- Point of intersection test and minimal distance test: look for intersecting lines in the decay volume and find the minimal distance in the third dimension
- Final test: remind the computer which coordinates were the correct ones and compare them to the ones chosen via track reconstruction evaluation

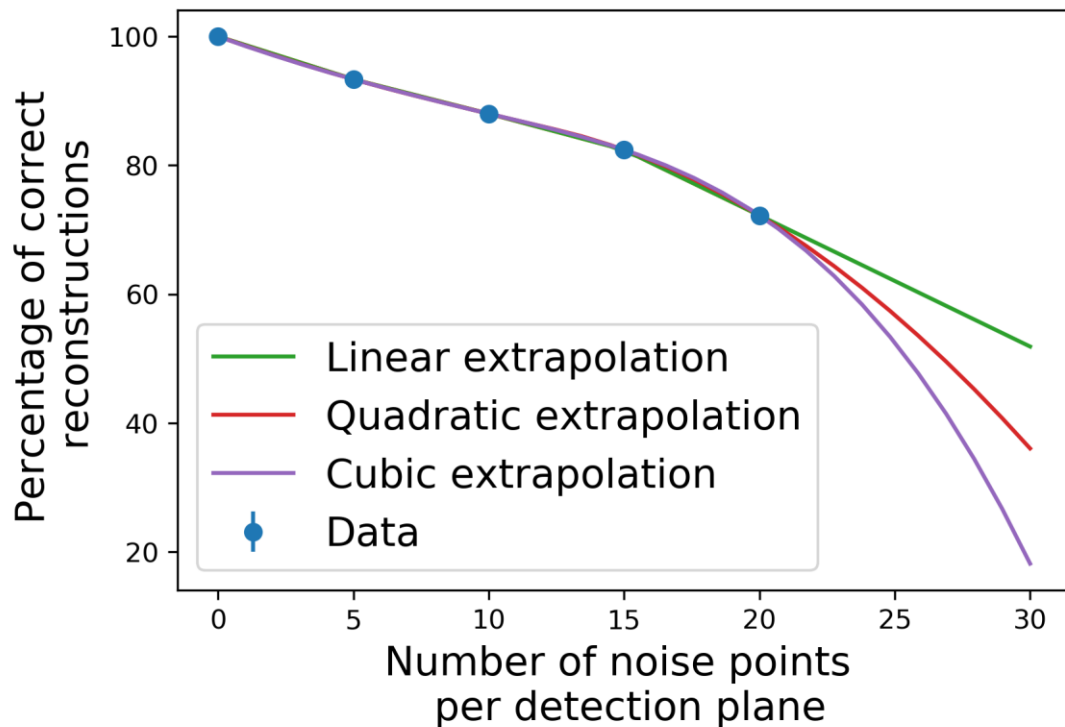


Least-squares fitting of a straight line in between “observed” data points. Taken from https://www.jmp.com/en_ca/statistics-knowledge-portal/what-is-regression/the-method-of-least-squares.html.

$$\sum e_{line_j}^2 = \sum (y_{observed} - y_{predicted})^2$$

Results

- Vertex reconstruction resolution: ± 2 cm
- Vertex reconstruction efficiency: 100 % for zero noise points, ~98.5 % on average between 0 and 50 noise points total, and ~92 % average between 0 and 150 noise points total.



Vertex reconstruction algorithm efficiency results for, 0, 5, 10, 15, and 20 noise points per detection plane for fixed angles.

Detecting EDMs with MAPP

- Frank, *et. al* [1] explore the possibility of detecting an anomalously large EDM with the MoEDAL-MAPP detector
- Revising previous results by Sher [6, 7] leads [1] to conclude that the energy loss of the EDM is

$$\frac{dE}{dx} = \pi n_e \frac{e^2}{4 \pi \epsilon_0} D \gamma$$

- New result:

$$-\frac{dE}{dx} = \left(\frac{k e^2 p^2 \pi^3 n_e}{2 v^2 m_e} \right) \left(4 \pi \epsilon_0 \frac{2 m_e \gamma v^2}{\pi e p} - \frac{\langle \omega \rangle^2}{\gamma^2 v^2} \right)$$

- High velocity regime:

$$\frac{-\frac{dE_A}{dx}}{-\frac{dE_S}{dx}} = \pi$$

ω = frequency of motion of the electronic binding;

$p = eD$ = electric dipole [$e * \text{cm}$]; m_e = magentic dipole; n_e = electron number density; $k = \frac{1}{4 \pi \epsilon_0}$

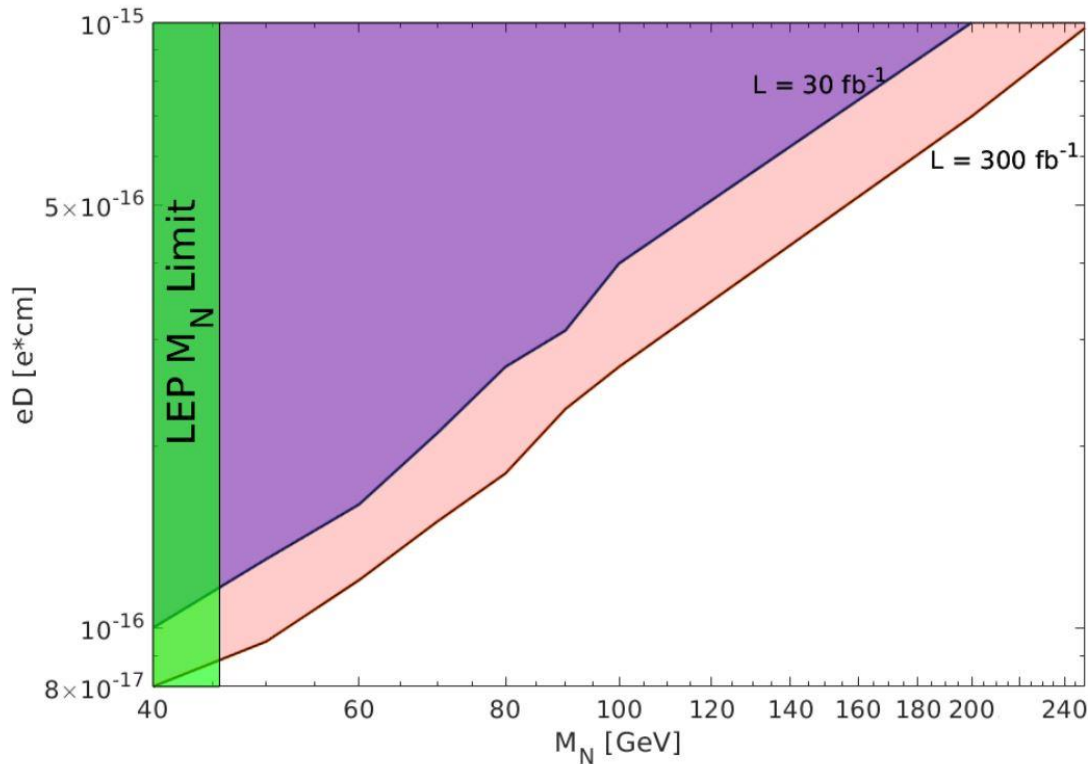
[1] M. Frank, M. de Montigny, P.-P. Ouimet, J.L. Pinfold, A. Shaa, and M. Staelens. “Searching for heavy neutrinos with the MoEDAL-MAPP detector at the LHC”. In: *Physics Letters B* 802(2020), p. 135204. Doi: 10.1016/j.physletb.2020.135204

[6] M. Sher and S. Nie. “Large Electric Dipole Moments of Heavy Neutrinos”. In: *Physical Review D* 65(093018) (May 21, 2002). doi: 10.1103/physrevd.65.093018

[7] M. Sher and J.R. Stevens. “Detecting a heavy neutrino electric dipole moment at the LHC”. In: *Physics Letters B* 777 (2018), pp. 246–249. issn: 0370-2693. Doi: <https://doi.org/10.1016/j.physletb.2017.12.022>

Detecting EDMs with MAPP (continuation)

- We assume that an anomalously large EDM could be detected if it gives rise to 100 photons or more in each of the 4 sections of the detector (totaling at least 400 photons). To convert energy deposition into number of photons in the scintillator, we assume that 10^4 photons are produced per MeV of energy deposited in the plastic scintillator [1, 8]



The reach for EDM detection at MoEDAL's MAPP detector at $\sqrt{s} = 14$ TeV, with 3 or more events observed at 95% C.L., and 30 fb^{-1} and 300 fb^{-1} of integrated luminosity. Taken from [1]

Conclusion

1) MAPP-1

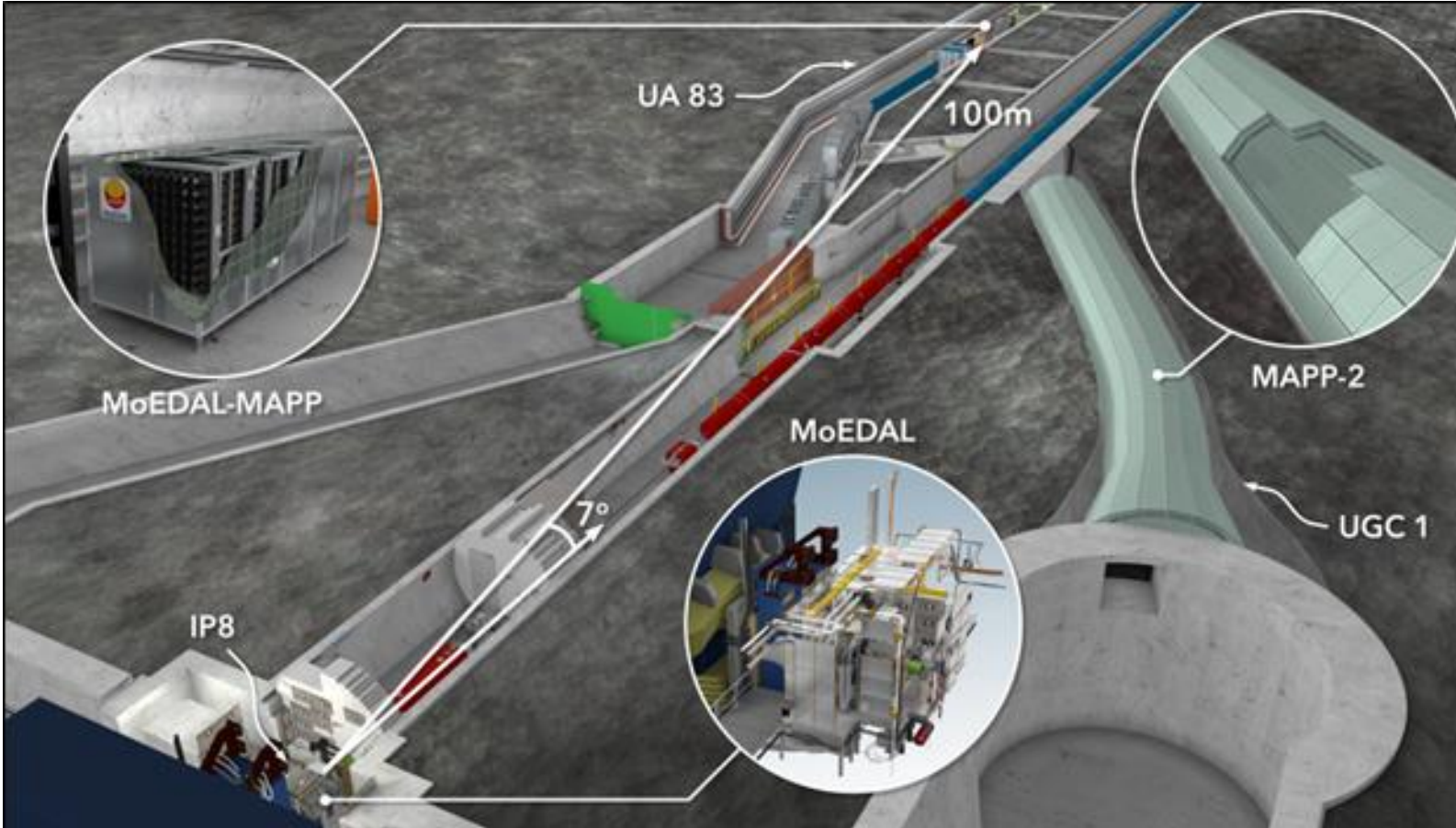
- Designed the procedure of polishing and wrapping the scintillator bars
- Designed the housing to create the coupling between the bar, the lightguide and the PMT
- Designed the procedure of installing the lightguides onto the bars
- Produced testing tile for veto (with embedded WLS fibres)
- Testing of the PMTs

2) MAPP-2

- Produced preliminary testing elements for MAPP-2: scintillating sheets with optical fibres embedded in it
- Created a mechanism to hold the SiPMs and fibres in contact
- Designed and ran a noise study on SiPMs put in coincidence
- Created a test algorithm for the eventual software development for the vertexing of MAPP-2 at the LHC

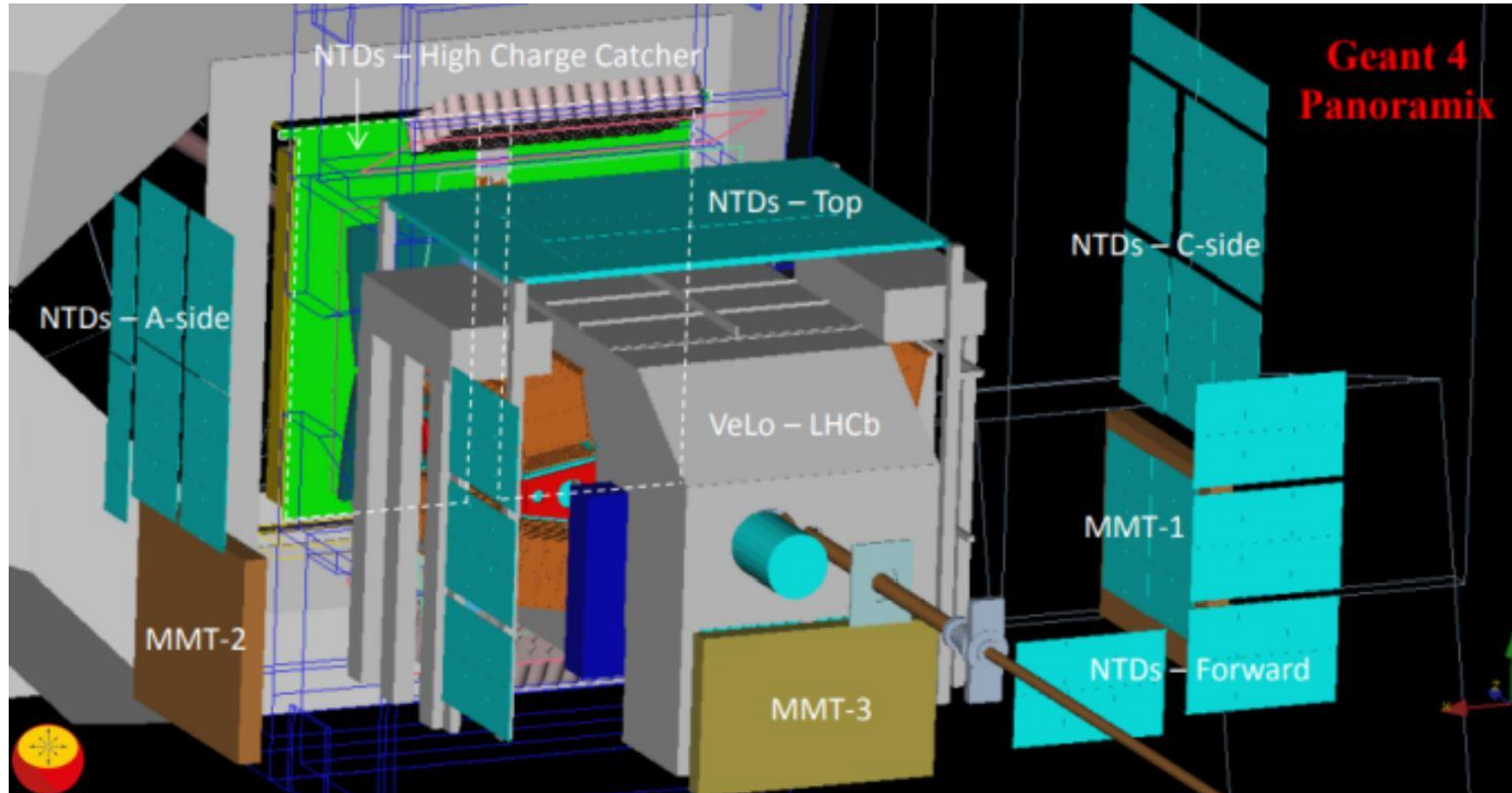
3) Participated in the re-calculation of the energy loss of an EDM as it passes through the scintillating material

Locations of MoEDAL, MAPP-1, and MAPP-2



Location of the MAPP detector(s) at the LHC. MAPP is to be installed in the UA83 (Phase-1) and UGC1 (Phase-2) tunnels at the LHC, which is adjacent to the MoEDAL detector

MoEDAL Geant4 Simulation Diagram

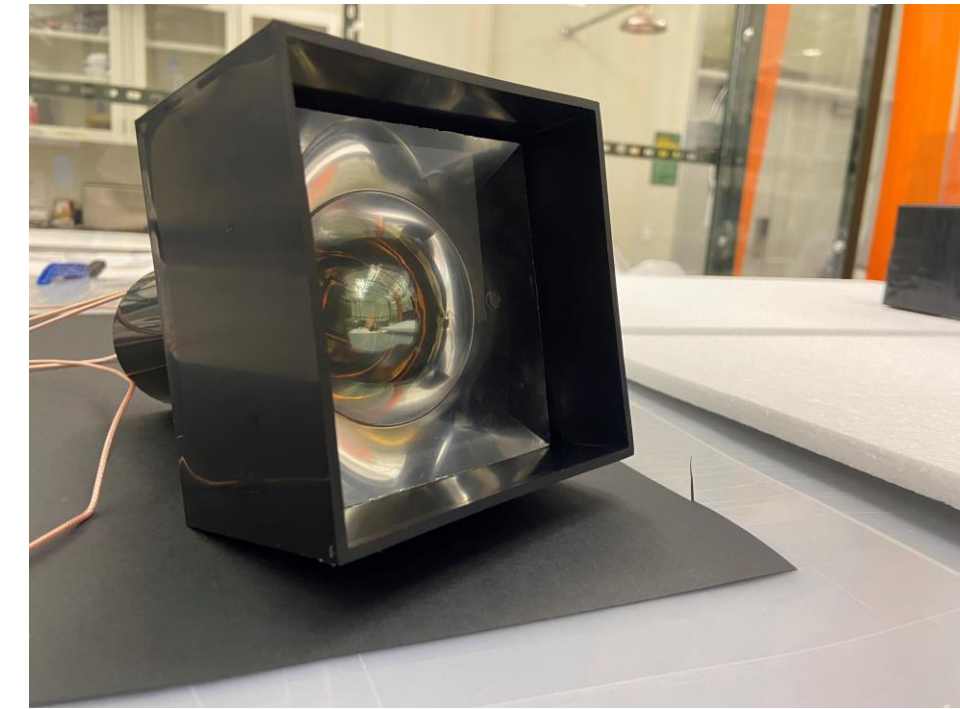


Simulation diagram of the MoEDAL detector in Geant4

Fully assembled scintillating unit for MAPP-1



Completed bar



PMT, lightguide, and housing
assembled

mCPs

- MoEDAL is studying mini-charged particles that are generated in a “model-independent” scenario [10,11] in which a new massless $U'(1)$ Abelian gauge field and a dark photon A'_μ couple to $B^{\mu\nu}$, a SM hyper-charge gauge field [10]. In addition, one adds from Dark QCD a massive dark fermion, $\psi_{mCP} m$, which has a mini-charged mass, m_{mCP} , that couples to the dark photon gauge field, A'_μ , charged with e' . Introducing an arbitrary parameter and a redefinition of the dark photon field to $A'_\mu \Rightarrow A'_\mu + \kappa B_\mu$, one obtains the interaction Lagrangian [10]:

$$\mathcal{L} = \mathcal{L}_{SM} - \frac{1}{4} A'_{\mu\nu} A'^{\mu\nu} + i\bar{\psi} (\partial + ie' A' - i\kappa e' B + im_{mCP}) \psi$$

- The fractional charged, expressed in terms of electric charge is given by $\epsilon = \kappa e' \cos(\theta_W) / e$

- [10] M. Staelens. The Search for New Physics at the LHC with the MoEDAL-MAPP Detector and an Investigation of Emergent Magnetic Monopole Like Excitations in an Exotic Condensed Matter System. PhD thesis, University of Alberta, 2021
- [11] A. Haas, C.S. Hill, E. Izaguirre, and I. Yavin. «Looking for milli-charged particles with a new experiment at the LHC». English (US). In: Physics Letters, Section B: Nuclear, Elementary Particle and High-Energy Physics 746 (June 2015), pp. 117–120. issn: 0370-2693. doi: 10.1016/j.physletb.2015.04.062



Looking for milli-charged particles with a new experiment at the LHC

Andrew Haas ^a, Christopher S. Hill ^b, Eder Izaguirre ^{c,*}, Itay Yavin ^{c,d}

^a Department of Physics, New York University, New York, NY, USA

^b Department of Physics, The Ohio State University, Columbus, OH, USA

^c Perimeter Institute for Theoretical Physics, Waterloo, ON, Canada

^d Department of Physics, McMaster University, Hamilton, ON, Canada

ARTICLE INFO

Article history:

Received 11 February 2015

Received in revised form 22 April 2015

Accepted 27 April 2015

Available online 30 April 2015

Editor: A. Ringwald

ABSTRACT

We propose a new experiment at the Large Hadron Collider (LHC) that offers a powerful and model-independent probe for milli-charged particles. This experiment could be sensitive to charges in the range $10^{-3}e$ – $10^{-1}e$ for masses in the range 0.1 – 100 GeV, which is the least constrained part of the parameter space for milli-charged particles. This is a new window of opportunity for exploring physics beyond the Standard Model at the LHC. The key new ingredients of the proposal are the identification of an optimal location for the detector and a telescopic/coincidence design that greatly reduces the background.

© 2015 The Authors. Published by Elsevier B.V. This is an open access article under the CC BY license (<http://creativecommons.org/licenses/by/4.0/>). Funded by SCOAP³.

it relies *only* on the production and detection of mCPs through their QED interactions.

We base the estimates for the potential reach of our proposed experiment on a particular theoretical framework, which we now briefly describe. While it is possible to simply add mCP particles to the Standard Model (SM), this is both unappealing from a theoretical point of view and strongly constrained by early Universe over-production of these particles (see [2,3,12,13] and references therein). A more appealing possibility is the existence of an extra abelian gauge field that couples to a massive Dirac fermion (“dark QED”) and that mixes with hypercharge through the kinetic term [14],

$$\begin{aligned} \mathcal{L} = & \mathcal{L}_{SM} - \frac{1}{4} A'_{\mu\nu} A'^{\mu\nu} + i\bar{\psi} (\partial + ie' A' + iM_{mCP}) \psi \\ & - \frac{\kappa}{2} A'_{\mu\nu} B^{\mu\nu}. \end{aligned} \quad (1)$$

Here ψ is a Dirac fermion of mass M_{mCP} that is charged under the new $U(1)$ field A'_μ with charge e' , and the field-strength is defined as $A'_{\mu\nu} = \partial_\mu A'_\nu - \partial_\nu A'_\mu$. The last term in Eq. (1) is a kinetic mixing term between the field strength of the new gauge boson and that of hypercharge. Such a term is expected in grand unified theories and more generally whenever there exist massive fields that are charged under both hypercharge and the new gauge boson, even when these heavy fields are not accessible at low energies.

Eliminating the mixing term by redefining the new gauge boson as $A'_\mu \rightarrow A'_\mu + \kappa B_\mu$ results in a coupling of the charged matter field ψ to hypercharge (as well as an immaterial redefinition of the hypercharge coupling).

* Corresponding author.

E-mail address: eder@pitp.ca (E. Izaguirre).

<http://dx.doi.org/10.1016/j.physletb.2015.04.062>

0370-2693/© 2015 The Authors. Published by Elsevier B.V. This is an open access article under the CC BY license (<http://creativecommons.org/licenses/by/4.0/>). Funded by SCOAP³.

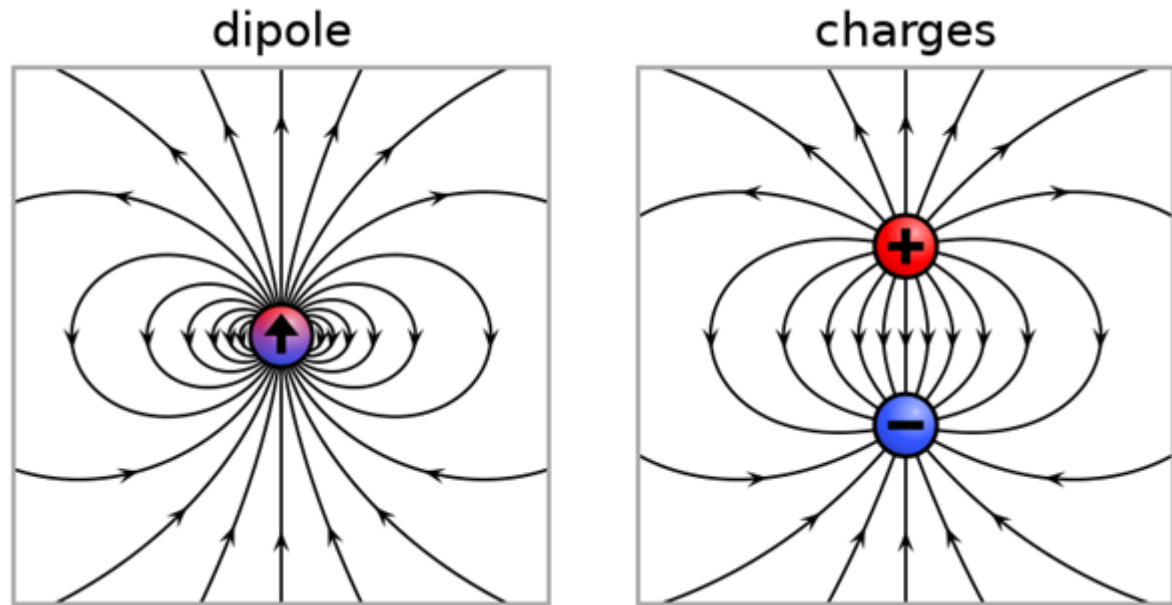
EDMs Classical Scenario

- Measure of the separation of positive and negative electrical charges in a system [12]. Could be two point charges or a charge distribution. It is given by, for two point charges and for a charge distribution, respectively:

$$P = qd$$

$$\mathbf{p}(\mathbf{r}) = \int_V \rho(\mathbf{r}') (\mathbf{r}' - \mathbf{r}) d^3 r'$$

- p = EDM magnitude;
- q = point charge magnitude
- d = distance between the two point charges
- ρ = charge density function;
- \mathbf{r} = vector between point charges in a volume V



(LEFT) point dipole. (RIGHT) dipole from two separated point charges. Taken from [11]

EDMs QM Scenario

- (Electron Case) Dirac particles couple to photons in form different ways, i.e., they have four different form factors arising from the matrix element of the electromagnetic current operator O^μ between two on-shell states [13,14]:

$$\bar{u}(\mathbf{p}_1)O^\mu u(\mathbf{p}_2) = \bar{u}(\mathbf{p}_1) \left\{ F_1(q^2)\gamma^\mu + \frac{i\sigma^{\mu\nu}}{2m} q_\nu F_2(q^2) + i\epsilon^{\mu\nu\alpha\beta} \frac{\sigma_{\alpha\beta}}{4m} q_\nu F_3(q^2) + \frac{1}{2m} \left(q^\mu - \frac{q^2}{2m} \gamma^\mu \right) \gamma_5 F_4(q^2) \right\} u(\mathbf{p}_2)$$

Non-relativistic limit:

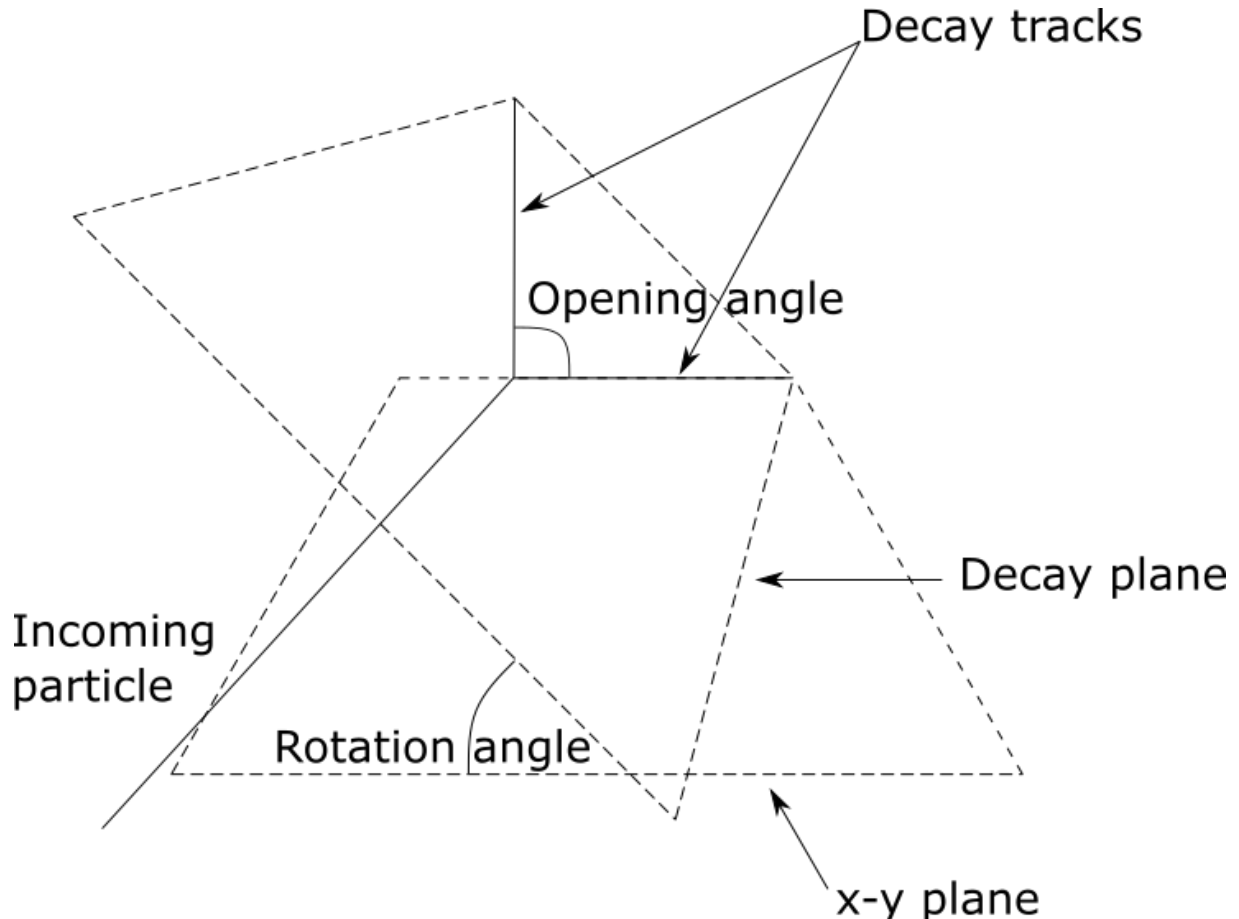
$$\begin{aligned} F_1(0) &= Q \text{ (charge)} \\ \frac{1}{2m}[F_1(0) + F_2(0)] &= \mu \text{ ([static]magnetic moment)} \\ -\frac{1}{2m}F_3(0) &= d \text{ (electric dipole moment)} \\ F_5(0) &= \text{Zeldovich anapole} \end{aligned}$$

$u(p_i)$ and $u(p_f)$ are 4-spinor solutions to the Dirac equation normalized so that $\bar{u}u = 2m_e$, $q^\mu = p_f^\mu - p_i^\mu$ is the momentum transfer from the current to the electron.

[13] Nowakowski, M.; Paschos, E.A.; Rodriguez, J.M. "All electromagnetic form factors". European Journal of Physics, 26(4) (April 14, 2005). Doi: 10.1088/0143-0807/26/4/001

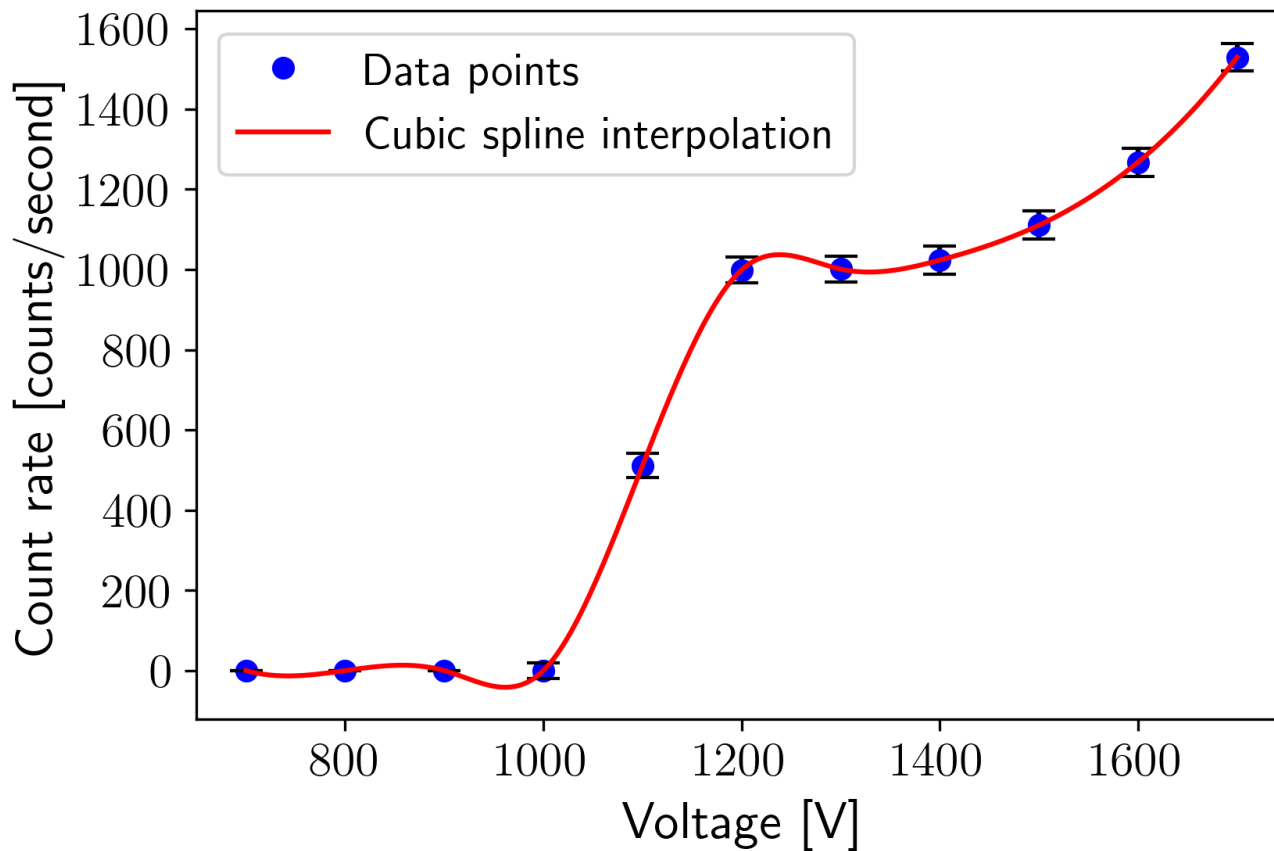
[14] Wikipedia. *Electron Electric Dipole Moment*. Retrieved from: https://en.wikipedia.org/wiki/Electron_electric_dipole_moment

Opening and Rotation Angles Definitions

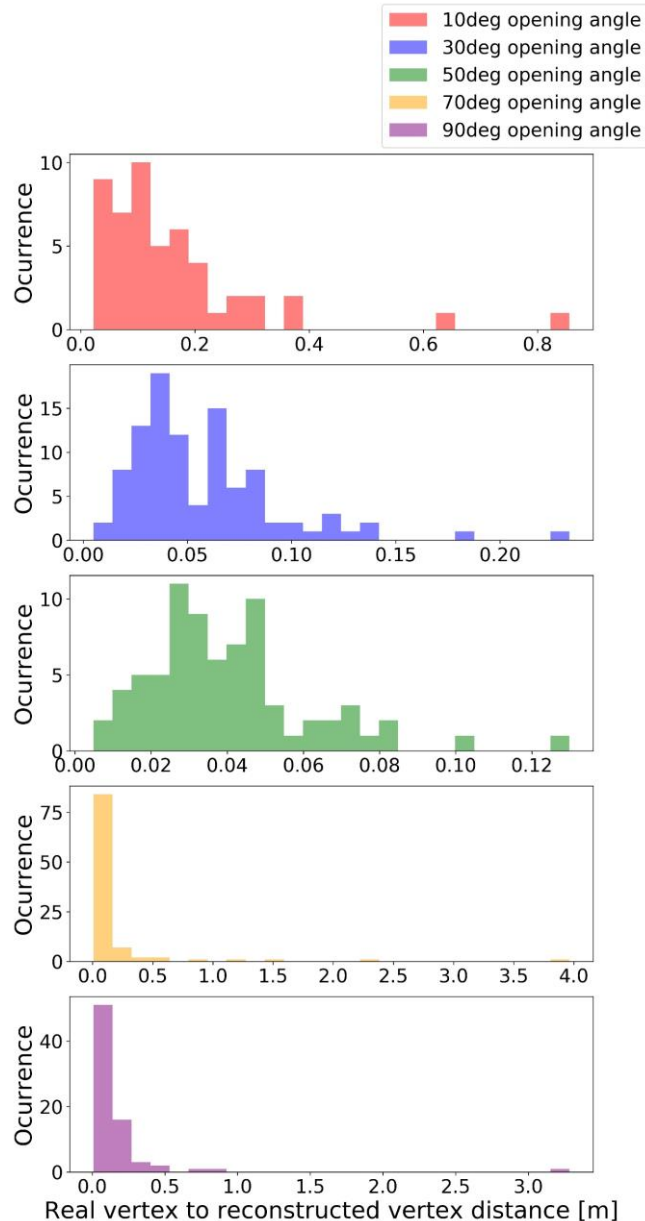


Opening and rotation angles in the vertexing simulation

HV Curve Above with Noise



HV curve for a PMT with voltages surpassing the plateau region



Histogram of the data generated for the distance between the reconstructed vertices to the coordinate system's origin.

3 Comparing Results

Let us compare the result we obtained in Section 3 with the result obtained by Sher et al [3]. First, let us massage the result obtained by Sher into something we can understand easily. Letting $p = eD$, we have,

$$\Delta E = \frac{1}{2m_e} \frac{1}{v^2 b^4} \frac{e^2 p^2}{(4\pi\epsilon_0)^2} \quad (38)$$

Considering a volume element $dV = 2\pi bdbdx$ and an electron number density n_e , we have (analogous to Equation 39),

$$-\frac{dE}{dx} = \Delta E n_e (2\pi bdb) \quad (39)$$

We integrate the impact parameter b from b_{min} to b_{max} . We have,

$$\begin{aligned} -\frac{dE}{dx} &= \frac{1}{(4\pi\epsilon_0)^2} \frac{\pi e^2 p^2 n_e}{m_e v^2} \int_{b_{min}}^{b_{max}} \frac{1}{b^3} db \\ &= \frac{1}{(4\pi\epsilon_0)^2} \frac{\pi e^2 p^2 n_e}{m_e v^2} (b_{min}^{-2} - b_{max}^{-2}) \end{aligned} \quad (40)$$

With $b_{min} = \frac{ep}{2m\gamma v^2} \frac{1}{4\pi\epsilon_0}$ and $b_{max} = \infty$, we have,

$$-\frac{dE}{dx} = \frac{\pi e p \gamma n_e}{4\pi\epsilon_0} \quad (41)$$

Let us compare the two derivations for energy loss of an electric dipole in Equation 45 and Equation 49 by taking the ratio. Massaging Equation 45 into a form easier for comparison, we have,

$$\begin{aligned} -\frac{dE}{dx} &= \left(\frac{ke^2 p^2 \pi^3 n_e}{2v^2 m_e} \right) \left(4\pi\epsilon_0 \frac{2m_e \gamma v^2}{\pi e p} - \frac{\langle \omega \rangle^2}{\gamma^2 v^2} \right) \\ &= \frac{\pi^2 e p n_e \gamma}{4\pi\epsilon_0} \left(1 - \frac{1}{4\pi\epsilon_0} \frac{\pi e p}{2m_e} \frac{\langle \omega \rangle^2}{\gamma^3 v^4} \right) \end{aligned} \quad (42)$$

Denoting Equation 50 by $-\frac{dE_A}{dx}$ and Equation 49 by $-\frac{dE_S}{dx}$, we have,

$$\frac{-\frac{dE_A}{dx}}{-\frac{dE_S}{dx}} = \pi \left(1 - \frac{1}{4\pi\epsilon_0} \frac{\pi e p}{2m_e} \frac{\langle \omega \rangle^2}{\gamma^3 v^4} \right) \quad (43)$$

By Equation 23, we have that $p = \frac{vm}{c}$.

$$\frac{-\frac{dE_A}{dx}}{-\frac{dE_S}{dx}} = \pi \left(1 - \frac{1}{4\pi\epsilon_0} \frac{\pi e m}{2m_e c} \frac{\langle \omega \rangle^2}{\gamma^3 v^3} \right) \quad (44)$$

Let us consider two regimes - low velocity and extremely high velocity. As $v \rightarrow \infty$, $\gamma \rightarrow \infty$ and $\frac{1}{\gamma^3 v^3} \rightarrow 0$. Therefore, in the high velocity regime, the ratio boils down to

$$\frac{-\frac{dE_A}{dx}}{-\frac{dE_S}{dx}} = \pi \quad (45)$$

The low velocity regime is a little harder. Substituting $e = 1.6 \times 10^{-19} C$, $\epsilon_0 = 8.85 \times 10^{-12}$, $m_e = 9.11 \times 10^{-31} kg$ into Equation 52,

$$\frac{-\frac{dE_A}{dx}}{-\frac{dE_S}{dx}} = \pi \left(1 - 8.2689 \times 10^{12} \frac{m \langle \omega \rangle^2}{\gamma^3 v^3} \right) \quad (46)$$

We now need to estimate the value of $\langle \omega \rangle$ and m .



Searching for heavy neutrinos with the MoEDAL-MAPP detector at the LHC



Mariana Frank^a, Marc de Montigny^{b,*}, Pierre-Philippe A. Ouimet^c, James Pinfold^d, Ameir Shaa^d, Michael Staelens^d

^a Department of Physics, Concordia University, Montreal, Quebec, H4B 1R6, Canada

^b Faculté Saint-Jean, University of Alberta, Edmonton, Alberta, T6C 4C9, Canada

^c Department of Physics, University of Regina, Regina, Saskatchewan, S4S 0A2, Canada

^d Department of Physics, University of Alberta, Edmonton, Alberta, T6G 2E1, Canada

ARTICLE INFO

Article history:

Received 30 November 2019

Received in revised form 2 January 2020

Accepted 6 January 2020

Available online 9 January 2020

Editor: G.F. Giudice

Keywords:

Heavy neutrino

Electric dipole moment

Heavy lepton

LHC

MilliQan

MoEDAL

ABSTRACT

We present a strategy for searching for heavy neutrinos at the Large Hadron Collider using the MoEDAL Experiment's MAPP detector. We hypothesize the heavy neutrino to be a member of a fourth generation lepton doublet, with the electric dipole moment (EDM) introduced within a dimension-five operator. In this model the heavy neutrino is produced in association with a heavy lepton. According to our current experimental and theoretical understanding, the electric dipole moment of this heavy neutrino may be as high as 10^{-15} e cm. Taking advantage of the sensitivity of MoEDAL detector, we examine the possibility of detecting such a heavy neutrino in the MAPP as an apparently fractionally charged particle, via ionization due to the neutrino's EDM.

© 2020 The Authors. Published by Elsevier B.V. This is an open access article under the CC BY license (<http://creativecommons.org/licenses/by/4.0/>). Funded by SCOAP³.